WILEY-BLACKWELL

Cladistics 37 (2021) 1–35

Cladistics

10.1111/cla.12416

Ultra-Conserved Elements and morphology reciprocally illuminate conflicting phylogenetic hypotheses in Chalcididae (Hymenoptera, Chalcidoidea)

Astrid Cruaud[a,†], Gérard Delvare[a,b,†], Sabine Nidelet[a], Laure Sauné[a], Sujeevan Ratnasingham[c], Marguerite Chartois[a], Bonnie B. Blaimer[d], Michael Gates[e], Seán G. Brady[f], Sariana Faure[g], Simon van Noort[h,i], Jean-Pierre Rossi[a] and Jean-Yves Rasplus[a,*]

[a]*CBGP, CIRAD, INRAe, IRD, Montpellier SupAgro, Université de Montpellier, Montpellier, France;* [b]*UMR CBGP, CIRAD, F-34398, Montpellier, France;* [c]*Centre for Biodiversity Genomics, University of Guelph, Guelph, ON, Canada;* [d]*North Carolina State University, Raleigh, NC, USA;* [e]*USDA, ARS, SEL, c/o Smithsonian Institution, National Museum of Natural History, Washington, DC, USA;* [f]*Department of Entomology, Smithsonian Institution, National Museum of Natural History, Washington, DC, USA;* [g]*Department of Zoology and Entomology, Rhodes University, Grahamstown, South Africa;* [h]*Research and Exhibitions Department, South African Museum,Iziko Museums of South Africa, PO Box 61, Cape Town, 8000, South Africa;* [i]*Department of Biological Sciences, University of Cape Town, Private Bag, Rondebosch, 7701, Cape Town, South Africa*

Accepted 15 February 2020

Abstract

Recent technical advances combined with novel computational approaches have promised the acceleration of our understanding of the tree of life. However, when it comes to hyperdiverse and poorly known groups of invertebrates, studies are still scarce. As published phylogenies will be rarely challenged by future taxonomists, careful attention must be paid to potential analytical bias. We present the first molecular phylogenetic hypothesis for the family Chalcididae, a group of parasitoid wasps, with a representative sampling (144 ingroups and seven outgroups) that covers all described subfamilies and tribes, and 82% of the known genera. Analyses of 538 Ultra-Conserved Elements (UCEs) with supermatrix (RAxML and IQTREE) and gene tree reconciliation approaches (ASTRAL, ASTRID) resulted in highly supported topologies in overall agreement with morphology but reveal conflicting topologies for some of the deepest nodes. To resolve these conflicts, we explored the phylogenetic tree space with clustering and gene genealogy interrogation methods, analyzed marker and taxon properties that could bias inferences and performed a thorough morphological analysis (130 characters encoded for 40 taxa representative of the diversity). This joint analysis reveals that UCEs enable attainment of resolution between ancestry and convergent/divergent evolution when morphology is not informative enough, but also shows that a systematic exploration of bias with different analytical methods and a careful analysis of morphological features is required to prevent publication of artifactual results. We highlight a GC content bias for maximum-likelihood approaches, an artifactual mid-point rooting of the ASTRAL tree and a deleterious effect of high percentage of missing data (>85% missing UCEs) on gene tree reconciliation methods. Based on the results we propose a new classification of the family into eight subfamilies and ten tribes that lay the foundation for future studies on the evolutionary history of Chalcididae.

Introduction

At a time when biodiversity studies are of critical importance (Dirzo et al., 2014; Hallmann et al., 2017), efforts made to resolve the tree of life are unequal between the different groups of organisms. In animals,

*Corresponding author:
E-mail address: jean-yves.rasplus@inra.fr
†Equal contributors.

most attempts using pangenomic data focus on vertebrates, for which past research has provided a solid framework based on external morphology, anatomy, biology and fossils (Titley et al., 2017). Many teams continuously add to our knowledge of vertebrate groups by performing phylogenomic studies to test previous hypotheses and resolve long-standing taxonomic disputes. When it comes to invertebrate groups, specifically to insects, which are the most speciose terrestrial organisms (Foottit and Adler, 2009), the picture is quite different. Background knowledge is poor for most groups, essentially based on a small number of morphological features, and only a few phylogenomic hypotheses using representative but limited sampling have been published at the family level. This is certainly a consequence of the so-called taxonomic impediment (Ebach et al., 2011; Wägele et al., 2011), difficulty in adapting to new technologies, and the inherent complexity of working with hyperdiverse groups. Obtaining a representative taxon sampling is problematic as new species and genera are constantly discovered, whereas some of the described taxa have only been found once. In addition, sampling is complicated by the recent restrictive access regulations to reduce the risk of supposed biopiracy (Prathapan et al., 2018). Finally, in many groups, species complexes do exist that are difficult to untangle based on morphology alone. Consequently, to avoid mixing closely related species, pangenomic data must be obtained from single, often tiny specimens, which is technically challenging.

Parasitoid wasps and more precisely chalcidoid wasps (*c*. 500 000 species; Heraty et al., 2013) are hyperdiverse and poorly known groups. Chalcidoid wasps have a key functional role in the ecosystems (Godfray, 1994) because they naturally regulate populations of other insects. Consequently, they are frequently used as biological control agents (Consoli et al., 2010). However, families of chalcidoid wasps are understudied and only a few family-wide, Sanger-based and poorly resolved phylogenetic hypotheses with limited sampling have been published (Chen et al., 2004; Desjardins et al., 2007; Owen et al., 2007; Burks et al., 2011; Cruaud et al., 2012; Murray et al., 2013; Janšta et al., 2018). Consequently, classifications are still based on morphological characters, although morphological convergence due to similar biology is widespread (van Noort and Compton, 1996; Heraty et al., 2013).

By reducing stochastic errors, genome-scale data offer greater opportunities to better resolve phylogenetic relationships (Philippe et al., 2005). Phylogenomic trees are usually highly supported but high statistical support often is still confused with accuracy (Lartillot et al., 2007). However, as for limited-size datasets, when the strongest signal that emerges from the data is not the historical signal, models or methods can be misled and infer incorrect topologies with high support (systematic error; Swofford et al., 1996; Phillips et al., 2004). With the increase in the number of gene regions, the probability of observing conflicting signal between markers due to violation of model assumption also increases (Kumar et al., 2012; Philippe et al., 2017) and total evidence approaches can lead to incorrect yet highly supported trees. This is why it is crucial to interpret molecular results in the light of morphological and biological data to point out possible contradictions (Wiens, 2004). However, in the case of poorly known groups, a feedback on morphological features is not straightforward.

Here, we were interested in testing to what extent a total evidence approach using pangenomic data with or without knowledge on the morphology and biology of the target group could lead to artefactual results or fill knowledge gaps. We focused on Chalcididae (Delvare, 2017), a family of Chalcidoidea that comprises 1548 described species and 83 genera classified into six subfamilies and seven tribes (Noyes, 2019; Table 1). The family is found on all continents except the polar regions but has its greatest diversity in the tropics. Species diversity within genera varies greatly, and four genera (*Antrocephalus*, *Brachymeria*, *Conura, Hockeria*) represent more than half (54%) of the species diversity, whereas 65 genera (78%) comprise less than five described species. The evolutionary history of the Chalcididae has been the focus of a single study based on a limited sampling (22 taxa) and a few (34) morphological characters (Wijesekara, 1997b). Another morphological study has addressed relationships within two tribes (Wijesekara, 1997a). Currently, our knowledge of the infrafamilial relationships comes mainly from three analyses that have focused on the higher-level classification of Chalcidoidea using 18S and 28S ribosomal gene regions (Campbell et al., 2000: 11 taxa; Munro et al., 2011: 41 taxa) or morphology plus rRNA (Heraty et al., 2013: 25 taxa). In two of the three analyses, the family was retrieved as polyphyletic and infrafamilial relationships were never resolved. Although Chalcididae are understudied, they are among the best-documented chalcidoid wasps. Characters used in previous studies can serve as a starting point for a thorough morphological analysis. We chose to infer the molecular phylogeny of the family using Ultra-Conserved Elements (UCEs) and their flanking regions (Faircloth et al., 2012; McCormack et al., 2012), which are increasingly used to solve ancient and recent divergences in insects (Blaimer et al., 2015, 2016a; Faircloth et al., 2015; Bossert et al., 2017, 2019; Jesovnik et al., 2017; Prebus, 2017; Ward and Branstetter, 2017; Branstetter et al., 2017a, 2017b; Van Dam et al., 2017; Cruaud et al., 2019; Kieran et al., 2019).

Table 1
Current and new higher classification of the Chalcididae

Current classification (Noyes 2018)		New classification (this study)	
Subfamilies	Tribes	Subfamilies	Tribes
Chalcidinae	Brachymeriini	Brachymeriinae **stat.r.**	
	Phasgonophorini	Phasgonophorinae **stat.r.**	Phasgonophorini, Stypiurini **trib.n.**
	Chalcidini	Chalcidinae	Chalcidini*
Cratocentrinae		Cratocentrinae	
Dirhininae		Dirhininae	
Epitraninae		Epitraninae	
Haltichellinae	Haltichellini, Hybothoracini, Tropimeridini, Zavoyini	Haltichellinae	Belaspidiini **trib.n.,** Haltichellini, Hybothoracini, Notaspidiini **trib.n.,** Tropimeridini, Zavoyini
Smicromorphinae		Smicromorphinae	

*We must note that *Hovachalcis* Steffan is not included in our analysis as only one specimen is known but it may deserve a tribal status on its own in the subfamily Chalcidinae.

We sequenced UCEs from 144 ingroup and seven outgroup taxa, analyzed UCE/taxa properties, performed exploration of the phylogenetic tree space and used different analytical approaches to detect possible systematic bias and conflicts among gene regions. We interpreted results in the light of a thorough morphological analysis (130 characters encoded for 40 taxa representing all major lineages) to propose a new classification for the higher relationships within the family.

Materials and methods

Sampling for the molecular study

The dataset contained 144 ingroup taxa (Table S1). All subfamilies and tribes as well as 82% of the world genera were included in the analysis. At the beginning of our study, 83 genera of Chalcididae were considered as valid and two as *incertae sedis* (*Antrochalcis* Kieffer, 1910 and *Chalcitiscus* Ghesquière, 1946, a fossil genus). The within-tribe classification was not the purpose of this study and will be reviewed elsewhere. However, the examination of numerous specimens in several museums and personal collections, together with a review of the literature, suggested that we need to remove six genera from synonymy (*Eniacomorpha* Girault, *Hontalia* Cameron, *Invreia* Masi, *Pareniaca* Crawford, *Parinvreia* Steffan, *Peltochalcidia* Steffan). We also discovered seven new genera awaiting description. Thus, we now consider 94 genera of Chalcididae as valid, 77 of which were included in our study. Most missing genera are extremely rare, known mostly from the type series only. Relationships within the Chalcidoidea are unclear (Heraty et al., 2013), but morphological features (Lotfalizadeh et al., 2007) as well as preliminary results obtained with anchored hybrid enrichment and UCEs (in prep.) suggest that the Eurytomidae may be the sister family of the Chalcididae. As a consequence, five species of Eurytomidae representing three subfamilies, as well as two species of Cerocephalinae (that form a clade with Eurytomidae + Chalcididae in the chalcidoid tree from the anchored/UCE approach) were used as outgroups. We used dried specimens (35% of the samples), specimens kept in 75–96% EtOH (50%), as well as DNA extracts (15%) kept at −20°C for about the last 10 years. The oldest specimen was collected in 1951 although most specimens were collected in the last 20 years. The paratypes of two species: *Kopinata partirubra* Bouček, 1988 and *Chalcis vera* Bouček, 1974 housed in the Natural History Museum, London (NHMUK) also were included.

DNA extraction, library preparation and sequencing

DNA was extracted nondestructively and vouchers were subsequently remounted on cards. DNA was extracted using the Qiagen (Valencia, CA) DNeasy Blood and Tissue kit following the manufacturer's protocol with a few modifications detailed in Cruaud et al. (2019). Library preparation followed Cruaud et al. (2019). Briefly, input DNA was sheared to a size of *c*. 400 bp using the Bioruptor® Pico (Diagenode). End repair, 3′-end adenylation, adapters ligation and PCR enrichment were then performed with the NEBNext Ultra II DNA Library prep kit for Illumina (NEB). Adapters that contained amplification and Illumina sequencing primer sites, as well as a nucleotide barcode of 5 or 6 bp long for sample identification were used to tag samples. Pools of 16 samples were made at equimolar ratio. Each pool was enriched using the 2749 probes designed by Faircloth et al. (2015) using a MYbaits kit (Arbor Biosciences) and following the manufacturer's protocol. The hybridization reaction was run for 24 h at 65°C. Post-

enrichment amplification was performed on beads with the KAPA Hifi HotStart ReadyMix. The enriched libraries were quantified with Qubit, an Agilent Bioanalizer and quantitative (q)PCR with the Library Quantification Kit - Illumina/Universal from KAPA (KK4824). They were then pooled at equimolar ratio. Paired-end sequencing (2*300 bp) was performed on an Illumina MiSeq platform at UMR AGAP (Montpellier, France).

UCE data analysis (from raw reads to UCEs)

Quality control checks were performed on raw sequence data with FastQC v.0.11.2 (Andrews, 2010). Quality filtering and adapter trimming were performed with Trimmomatic-0.36 (Bolger et al., 2014). Overlapping reads were merged using FLASH-1.2.11 (Magoc and Salzberg, 2011). Demultiplexing was performed using a bash custom script (Cruaud et al., 2019). Assembly was performed with Trinity (Haas et al., 2013). UCE loci were identified with PhyluCE (Faircloth 2016) (*phyluce_assembly_match_contigs_to_probes*, *phyluce_assembly_get_match_counts --incomplete matrix*, *phyluce_assembly_get_fastas_from_match_counts*, all scripts were used with default parameters).

UCE data analysis (from UCEs to phylogenetic trees)

Those UCEs present in more than 70% of the taxa were retained for analysis. UCEs were aligned with MAFFT v.7.245 (-linsi option; Katoh and Standley, 2013). Sites with >50% gaps were removed from the alignments using the program seqtools implemented in the package PASTA (Mirarab et al., 2014b). Sequences exhibiting up to 500 gaps and ten substitutions in pairwise alignments between all members of a UCE set were flagged by a custom script (available from https://github.com/DNAdiversity/UCE-Cross-Contamination-Check) as potential contaminations and reviewed before exclusion in subsequent analysis. Individual gene trees were inferred with raxmlHPC-PTHREADS-AVX v.8.2.4 (Stamatakis, 2014). As α and the proportion of invariable sites cannot be optimized independently from each other (Gu et al., 1995) and following Stamatakis' personal recommendation (RAxML manual), the proportion of invariant sites was not included in the model. A rapid bootstrap search (100 replicates) followed by a thorough maximum-likelihood (ML) search (-m GTRGAMMA) was performed. TreeShrink (Mai and Mirarab, 2018) was used to detect and remove abnormally long branches in individual gene trees (e.g. due to misalignment). The per-species mode was used and preliminary analyses together with gene tree visualization showed that the optimal value of *b* (the percentage of tree diameter increasing from which a terminal should be removed) was 20. Indeed, as reported in the TreeShrink tutorial, lower values of *b* led to the removal of species even when they were not on particularly long branches. All other parameters were set to default values. Once outliers were removed, UCEs were re-aligned with Mafft-linsi and alignments were cleaned using seqtools. TreeShrink was used a second time to clean gene trees from long branches that might have been missed due to the presence of extra-long branches in the original gene trees. The per-species mode was used with *b* set to 20 but only the longest outliers were removed (*k* was set to 1). All other parameters were set to default values. Once outliers were removed, UCEs were re-aligned with Mafft-linsi and alignments were cleaned using seqtools.

The final dataset was analyzed using supermatrix and coalescent-based summary methods. Phylogenetic trees were estimated from the concatenated dataset using ML as implemented in raxmlHPC-PTHREADS-AVX v.8.2.4 (Stamatakis, 2014) and IQTREE v.1.5.3 (Nguyen et al., 2015). For the RAxML analysis, a rapid bootstrap search (100 replicates) followed by a thorough ML search (-m GTRGAMMA) was performed. IQTREE analysis employed an ML search with the GTR + G model with branch supports assessed with ultrafast bootstrap (Minh et al., 2013) and SH-aLRT test (Guindon et al., 2010; 1000 replicates). For both RAxML and IQTREE, two analyses were conducted: (i) on the unpartitioned dataset and (ii) on the dataset partitioned according to the best partitioning scheme inferred by PartitionFinder 2.1.1 (Lanfear et al., 2017) using the Sliding-Window Site Characteristics (SWSC) method. This method recently has been developed to account for within-UCE heterogeneity (conserved core vs. flanking, variable regions; Tagliacollo et al., 2018). To fit with RAxML models and as α and the proportion of invariable sites cannot be optimized independently from each other, only the GTR + G model was evaluated. Branch lengths were considered as linked, model selection and partitioning scheme comparison were performed with the corrected Akaike Information Criterion and the rclusterf algorithm. Finally, we used the GHOST model implemented in IQTREE to account for heterotachous evolution as it does not require *a priori* data partitioning, a possible source of model misspecification (Crotty et al., 2019). ASTRAL-III v.5.6.1 (Zhang et al., 2018) and ASTRID (Vachaspati and Warnow, 2015) were used to infer a species tree from the individual UCE trees inferred by RAxML. To improve accuracy (Zhang et al., 2018) nodes with bootstrap percentage (BP) support <10 were collapsed in individual gene trees with the perl script AfterPhylo.pl (Zhu, 2014). For the analysis with ASTRID and following recommendations for incomplete distance matrices, BioNJ was used to compute the phylogeny. Node

supports were evaluated with local posterior probabilities (local PP) for the ASTRAL tree and 100 multilocus bootstrapping (Seo, 2008) for the ASTRID tree. Summary statistics were calculated using AMAS (Borowiec, 2016). Tree annotation was performed with TreeGraph 2.13 (Stöver and Müller, 2010). Correlation analysis between properties of the UCEs was performed with the R package performance analytics (Peterson and Carl, 2018).

Exploration of topological conflicts in the molecular dataset

New approaches have recently been developed to identify markers/sites supporting conflicting topologies that either make explicit assumptions about the biological basis of conflict (e.g. horizontal transfer, incomplete lineage sorting (ILS), recombination, gene duplication) or not. Early approaches (e.g. Abby et al., 2010; Heled and Drummond, 2010; Szöllősi and Daubin, 2012) were computationally too intense to be implemented on large datasets. Furthermore, they are limited in their focus, constrained to one or two sources of incongruence and may not be robust to additional sources (Gori et al., 2016). Here, we used more recent approaches that do not rely on any assumptions about the biological basis of conflicts, and are computationally tractable on large datasets. This involves: partitioning of the data into coherent groups by clustering of tree to tree distances (Gori et al., 2016; Duchêne et al., 2018) or statistical tests of incongruence (Gene Genealogy Interrogation (GGI); Arcila et al., 2017; Zhong and Betancur-R, 2017; Betancur-R et al., 2019). For the clustering approach, geodesic distances between all pairs of trees were calculated with TreeCl (Gori et al., 2016), which requires overlapping sets of samples (= specimens/terminals) between trees but allows missing samples in trees. Then, the optimal number of clusters obtained with the Partitioning Around Medoids algorithm (Kaufman and Rousseeuw, 1990) was estimated with the gap statistics as implemented in the R package cluster (Maechler et al., 2018; R Core Team, 2018; K_{max} was set to 10 and number of bootstrap samples was set to 500 to keep computation time reasonable). The R package factoextra (Kassambara and Mundt, 2017) was used to visualize clusters (ggplot2-based scatter plot; Wickham, 2016). Possible effects of missing data or gap content were evaluated by testing whether these variables were phylogenetically clustered on any of the conflicting topologies. Tests were conducted using the K statistic (Blomberg et al., 2003) with the R package phytools 0.6-00 (Revell, 2012). The null expectation of K under no phylogenetic signal was generated by randomly shuffling the tips of the phylogeny 1000 times.

We also used GGI to compute the relative support of the UCEs for each competing topology following Arcila et al. (2017). RAxML was used to infer trees from UCEs using each of the three competing topologies (Fig. 1) as multifurcating constraints (the structure of the backbone was fixed, but taxa within clades were free to move around). Thus, three constrained trees were inferred from each UCE. Per-site log-likelihood scores for all constrained trees were calculated with RAxML and used to perform approximately unbiased (AU) tests (Shimodaira, 2002) in the package CONSEL (Shimodaira and Hasegawa, 2001). The program makermt was used to generate $K = 10$ sets of bootstrap replicates with each set consisting of 100 000 replicates of the row sums. For each UCE, constrained trees were ranked by P-values of the AU test. The constrained tree with the highest P-value was considered as the best explanation of the data.

Finally, we examined whether compositional heterogeneity among loci and nucleotide positions as well as evolutionary rate heterogeneity among taxa could explain topological conflict. GC content and long-branch (LB) score heterogeneity were calculated for each UCE and each taxon in all UCEs. GC content was calculated with AMAS (Borowiec, 2016) and LB heterogeneity scores were calculated with TreSpEx (Struck, 2014). In a given tree, the per sample LB score measures the percentage deviation of the patristics distance (PD) of a sample to all others, from the average PD across all samples (Struck, 2014). For a given tree, the LB score heterogeneity is the standard deviation of the LB scores of the samples present in the tree. Thus, the LB score heterogeneity reflects the branch length heterogeneity of a given tree and is independent of the root of the tree. Consequently, calculation of LB score heterogeneities can help to prevent possible Long Branch Attraction (LBA) artefacts (Phillips et al., 2004; Bergsten, 2005). Hierarchical clustering of taxa based on GC content and LB scores was performed with the R package cluster. The LBA artefact also was tested by removing outgroups from the analysis (Bergsten, 2005).

Morphological analyses: focus on the tentorium and its external landmarks

This study is the first in the superfamily Chalcidoidea to investigate the tentorium as a phylogenetic character and to establish the connection between the inner skeleton of the cephalic capsule and its external landmarks on the back of the head. This section describes the method used to examine and code the different bridges.

Phylogenetic informativeness of the characters of the head capsule in Hymenoptera was highlighted recently (Vilhelmsen, 2011; Burks and Heraty, 2015;

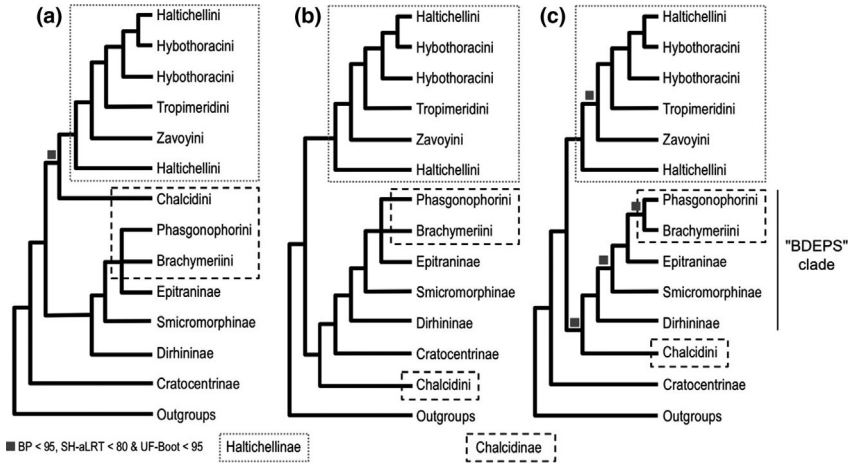

Fig. 1. Summary of the topologies recovered from the Ultra-Conserved Element (UCE) dataset. The current classification (Table 1) is used to annotate the trees. Nodes are collapsed when BP support or SH-aLRT/UFBoot supports <50. All nodes with BP > 95 and SH-aLRT > 80/UFBoot > 95 unless specified with a colored box. Topology (a) is observed when the complete UCE dataset is analyzed with concatenation approaches (RAxML, IQTREE, GHOST, with or without partition). The node grouping Chalcidini with Haltichellinae is supported by moderate BP support (<80) and low SH-aLRT/UFBoot supports (<80/<95). Other nodes are highly supported. Topology (b) is observed when the complete UCE dataset is analyzed with ASTRAL. All nodes are highly supported (localPP = 1.0). Topology (b) is also inferred when mid-point rooting instead of outgroup rooting is used to root the trees obtained with the concatenation approaches. Topology (c) is observed when the complete UCE dataset is analyzed with ASTRID. The node grouping Chalcidini with Dirhininae-Smicromorphinae-Epitraninae-Brachymeriini-Phasgonophorini is poorly supported (BP = 32). Topology (c) also is observed in about 20% of the bootstrap trees obtained with the concatenation approaches. Topology (c) is inferred with concatenation approaches when UCEs with GC content >0.48 or nucleotides with GC content >0.57 are removed from the dataset. In these cases, the node grouping Chalcidini with the Dirhininae-Smicromorphinae-Epitraninae-Brachymeriini-Phasgonophorini group is only moderately supported (BP = 67 and BP = 80). Topology (c) also is observed when the set of input gene trees for the ASTRAL analysis is reduced to trees for which ingroups are monophyletic. Current higher classification is used to annotate the trees. For brevity, the clade grouping Brachymeriini + Dirhininae + Epitraninae + Phasgonophorini + Smicromorphinae is the "BDEPS" clade throughout text.

Zimmermann and Vilhelmsen, 2016). However, interpretation is difficult and requires landmarks (Burks and Heraty, 2015). More precisely, the identity of the sclerotized structures between the occipital foramen and the oral fossa is still debated. The homology and nomenclature of these structures were established by Snodgrass (1928, 1942, 1960) and reassessed by Vilhelmsen (1999) and Burks and Heraty (2015). These authors describe various types of 'bridges', such as postgenal, hypostomal and subforaminal bridges, according to the cephalic part – postgena or hypostoma – from which they putatively originate. In his phylogenetic analyses of the Chalcididae, Wijesekara (1997a, 1997b) used the back of the head – reduced to a single character – and distinguished a 'hypostomal bridge' and a 'genal bridge'. As a detailed examination of the back of the head in the Eurytomidae (Lotfalizadeh et al., 2007), the probable sister group of the Chalcididae, provided useful characters for their phylogeny, we decided to investigate these characters in the Chalcididae. Chalcididae exhibits variable and puzzling structures that may be phylogenetically informative but necessitate a thorough identification of homologies among the subfamilies and more largely with other families of Chalcidoidea. Examination of the tentorium appeared to be the unique way to provide landmarks and additional characters.

In order to define the characters (and states) that would be informative to resolve phylogenetic relationships within Chalcididae and beyond, we worked on a subset of 16 Chalcididae (that were included in the whole morphological analysis) and 11 outgroups (two of which were included in the whole morphological analysis). The ingroup included at least one representative of each subfamily and tribe, namely: *Cratocentrus* aff. *decoratus* (Klug) (Cratocentrinae); *Stypiura* sp. and *Trigonura* sp. (Chalcidinae, Phasgonophorini); *Brachymeria minuta* (Linnaeus) and *B. tibialis* (Walker) (Chalcidinae, Brachymeriini); *Chalcis myrifex* (Sulzer), *Conura decisa* (Walker), *C. immaculata* (Cresson), *C. femorata* (Fabricius) and *Melanosmicra variventris* (Cameron) (Chalcidinae, Chalcidini); *Epitranus observator* Walker (Epitraninae); *Dirhinus anthracia* Walker (Dirhininae); *Hockeria bifasciata* Walker and *Antrocephalus* sp. (Haltichellini, Haltichellinae); *Notaspidium* sp. and *Invreia subaenea* Masi (Hybothoracini, Haltichellinae). The outgroups included *Leucospis dorsigera* Illiger (Leucospidae); *Macrorileya inopinata* (Silvestri) (Eurytomidae, Buresinae); *Tetramesa* sp., *Eurytoma crotalariae* Risbec and *Aximopsis collina* (Zerova) (Eurytomidae, Eurytominae); *Chalcedectus* sp. (Chalcedectini); *Cleonymus brevis* Bouček (Cleonymini) and *Lycisca* sp. (Lyciscini), all presently classified in Pteromalidae subfamily

Cleonyminae; *Norbanus* sp. and *Pteromalus* sp. (Pteromalidae, Pteromalinae) and *Glyphomerus stigma* (Fabricius) (Torymidae).

Specimens were prepared before examination using the following protocol. The maxilla and labium were removed and the head was fixed with water-soluble glue on a slide. A transverse section of the head was made with a razor blade. The posterior part of the head was then washed in water, cleared through immersion in potassium hydroxide at 10%, followed by washing with increasing concentrations of ethanol. The remaining tissues were removed in order to make only the tentorium visible. The head was finally fixed at the apex of a minutien pin for examination with a stereomicroscope. Imaging was made with a JVC KY-75U 3CCD digital camera attached to an EntoVision microscope and the stacked, serial images obtained were combined using CARTOGRAPH 5.6.0 (Microvision, Evry, France). Finally, we used a SEM microscope (Zeiss DSM 950, Zeiss, Oberkochen, Germany) for detailed examination and further imaging.

Zimmermann and Vilhelmsen (2016) defined and described in detail the structures of the tentorium; the nomenclature used in their paper is followed here. Examination of the tentorium provided evidence for defining the landmarks that were used to identify and name the external structures on the back of the head; here we mostly followed the nomenclature proposed by Burks and Heraty (2015) except that we interpret the external landmarks on the basis of the internal structure, which induces changes in interpretation of some external features (e.g. pits).

Clearing the head showed that the cuticle was not uniformly thick over its posterior part. The cuticle was thinner along the median strip of ornamentation (mso, list of abbreviations in Table 2) than on the postgena or the hypostoma. The relevant surface may therefore be identified as a different structure that constitutes a bridge. The lower-most bridge, situated below the dorsal level of the hypostomal carina, and receding in comparison with the surface of the postgena, is thus identified as the hypostomal bridge (hb). The surface delimited laterally by the posterior tentorial sulci (pts) is the subforaminal bridge (sfb). As the pts do not always reach ventrally the level of the upper limit of hypostoma, the transverse strip between the two surfaces may be hypothesized to be of postgenal origin. The median strip of ornamentation (mso), which is an extension of the subforaminal bridge (sfb), is thus formed of two parts: a broad dorsal surface delimited by pts and a narrow ventral surface reduced to the mso.

Following our observations, 26 characters and their corresponding character states were defined (characters 28–53 of the global list below, all illustrated in Figs 2, 3, 4, 5, 6, 7 and 8).

Table 2
Abbreviations used for the morphological analysis

ap	anterior process	[internal]
ata	anterior tentorial arm	[internal]
dta	dorsal tentorial arm	[internal]
fca	foraminal carina	[external]
fcy	foraminal cavity	[external]
ga	gena	[external]
ha	hypostoma	[external]
hb	hypostomal bridge	[external]
hc	hypostomal carina	[external]
hp	hypostomal process	[internal]
hpp	pit at dorsal end of hypostomal process	[external]
lb	labrum	[external and internal]
ll	lateral lamella of anterior tentorial arm	[internal]
mc	maxillary condyle	[external]
md	mandible	[external and internal]
mso	median strip of ornamentation	[external]
of	occipital foramen	[external and internal]
pg	postgena	[external and internal]
pgb	postgenal bridge	[external and internal]
pgg	postgenal groove	[external]
pgvd	postgenal ventral depression	[external]
pola	postoccipital lateral arm	[external]
polp	postoccipital lateral pit	[external]
polps	postoccipital lateral process	[external and internal]
pp	posterior process	[internal]
ppp*d*	pit at dorsal end of posterior process	[external]
ppp*v*	pit at ventral end of posterior process	[external]
pta	posterior tentorial arm	[internal]
ptp	posterior tentorial pit	[external]
pts	posterior tentorial sulcus	[external]
sfb	subforaminal bridge	[external and internal]
tb	tentorial bridge	[internal]
tbp	pit at lateral end of tentorial bridge	[external]

Morphological analyses: sampling and characters

A matrix of 130 characters was assembled for 40 species that covered all major lineages of the Chalcididae. Illustrations and historical context for characters and states can be found in the cited references. A list of abbreviations used in text is provided in Table 2.

1. **Metallic body color**. (0) present; (1) absent.
2. **Sclerotization of body**. (0) head and mesosoma moderately sclerotized, mostly reticulate or coriaceous, gaster slightly sclerotized, collapsing when dried; (1) head and mesosoma moderately sclerotized, mostly reticulate or coriaceous, gaster moderately sclerotized, not collapsing when dried; (2) head and mesosoma strongly sclerotized punctured and/or areolate, gaster distinctly sclerotized, not collapsing when dried (Delvare, 2017: cf. fig. 1); (3) head and mesosoma strongly sclerotized but

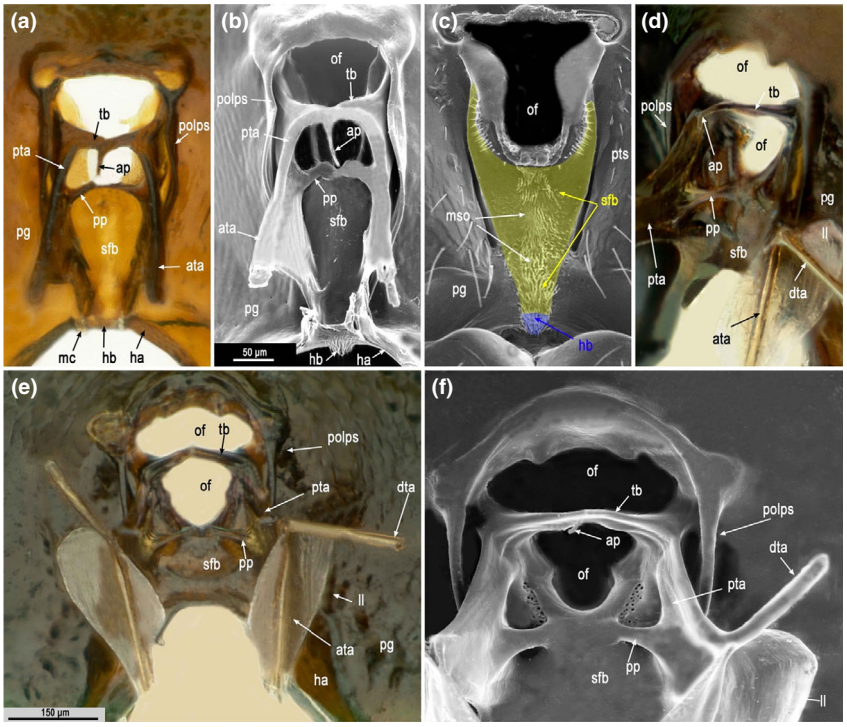

Fig. 2. Tentorial complex for outgroups (other Chalcidoidea). (a–c) *Glyphomerus stigma*; (d–f) *Chalcedectus* sp.; (a) subforaminal and hypostomal bridges anterior view; (b, d–f) Tentorium anterior view; (c) subforaminal and hypostomal bridges posterior view; (e) tentorium anterolateral view. Abbreviations in Table 2. [Colour figure can be viewed at wileyonlinelibrary.com]

metasoma collapsing when dried (Bouček, 1988: cf. fig. 100).

3. **Relation between labrum and clypeus.** (0) labrum overlapped by clypeus (Delvare et al., 2019: cf. fig. 21A); (1) labrum exposed and abutting anterior to clypeal margin, not overlapped by clypeus (Delvare, 2017: cf. fig. 12).
4. **Structure of labrum.** (0) lightly sclerotized, without sculpture on surface (Delvare et al., 2019: cf. fig. 21A); (1) plate-like, often with sculpture on surface (Delvare, 2017: cf. fig. 12).
5. **Labral setae.** (0) scattered across surface; (1) restricted to apical margin (Delvare, 2017: cf. fig. 81).
6. **Mandibular base.** (0) at least dorsally concealed by genal margin; (1) exposed, condyles elongate and visible externally, mouth margin not incised for reception of mandible (lateral to clypeus) (Delvare, 1992: cf. figs 54–66); (2) exposed, mouth margin thickened and incised for reception of dorsal corner of mandible (Abul-Sood et al., 2018: cf. fig. 3).
7. **Mouth margin above mandible.** (0) mouth margin not incised for reception of mandible; (1) mouth margin thickened and incised for reception of dorsal corner of mandible (Delvare, 2017: cf. fig. 12).
8. **Exposed muscle of mandible.** (0) below the exposed plane of the mandible and not extending into an incision; (1) on the same plane with mandible and extending into incision on outer surface of mandible (Abul-Sood et al., 2018: cf. fig. 3).
9. **Number of teeth on left mandible.** (0) three; (1) two; (2) four.
10. **Number of teeth on the right mandible.** (0) three; (1) two; (2) four.
11. **Length of mandibular teeth.** (0) ventral tooth about the same length as dorsal one; (1) ventral tooth much longer than dorsal one (Delvare, 2017: cf. fig. 116); (2) ventral tooth much shorter than dorsal one (Delvare, 1992: cf. fig. 54).
12. **Orientation of mandibular teeth.** (0) endodont (Delvare, 1992: cf. figs 54–66); (1) exodont (Delvare and Copeland, 2018: cf. fig. 7).
13. **Channel on posterior surface of mandible.** (0) absent; (1) present.
14. **Delimitation of upper margin of clypeus.** (0) impressed line (sulcus); (1) visible through change in sculpture; (2) step-like; (3) no evident limit.
15. **Lateral clypeal sulcus.** (0) present; (1) absent.
16. **Shape of clypeus.** (0) about as broad as long (Delvare and Copeland, 2018: cf. fig. 8); (1) >3 times as broad as long.

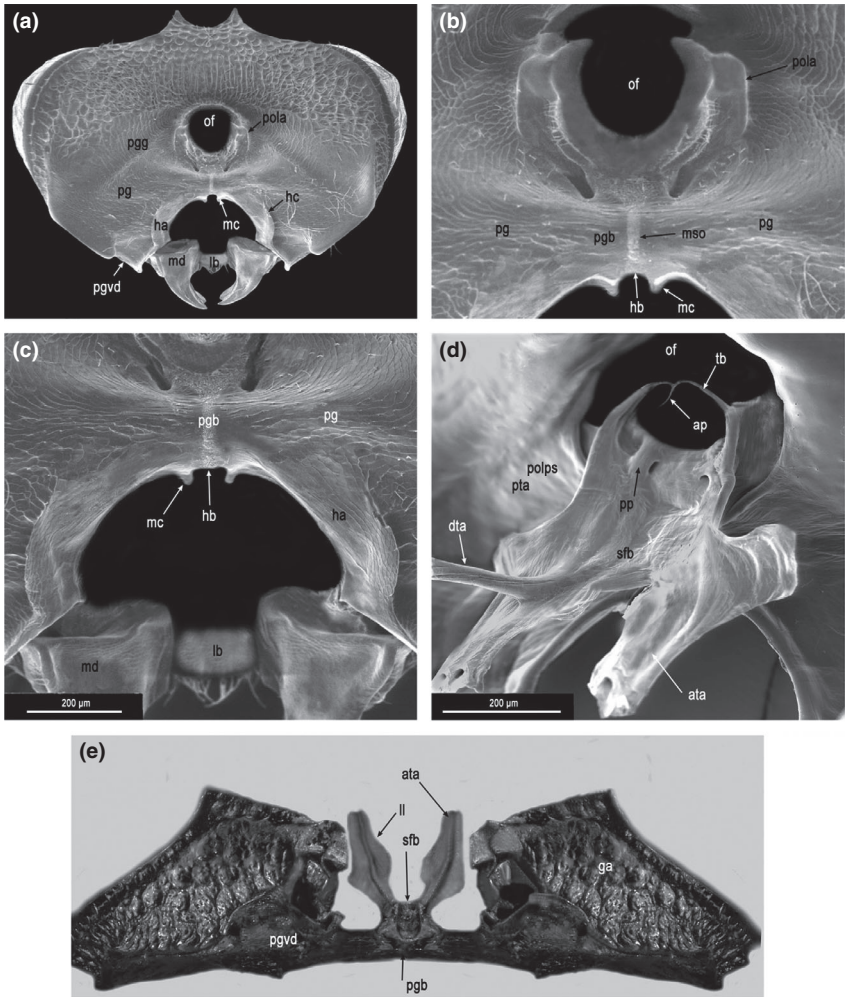

Fig. 3. Tentorial complex for Cratocentrinae, *Cratocentrus*. (a) Head posterior view; (b–c) postgenal bridge posterior view; (d) Tentorium anterodorsal view; (e) Tentorium ventral view. Abbreviations in Table 2.

17. **Position of toruli relative to oral cavity. (**0) ventral margin of torulus in lower third of face, not adjacent to clypeus (Delvare, 2017: cf. fig. 63); (1) near middle of head or higher; (2) adjacent to clypeus.
18. **Anterior tentorial pits.** (0) visible; (1) not visible externally.
19. **Malar sulcus.** (0) complete; (1) incomplete; (2) absent.
20. **Genal carina.** (0) absent; (1) angular but not carinate; (2) clearly present, raised (Delvare, 1992: cf. figs 460–467).
21. **Subapical genal tooth.** (0) postgena not depressed above oral fossa, genal tooth or protrusion absent; (1) postgena distinctly depressed above oral fossa, hence genal carina forming a protrusion at lateral corner of mouth; (2) postgena distinctly depressed above oral fossa, genal carina absent just above mouth corner, forming a tooth at some distance from it (Abul-Sood et al., 2018: cf. fig. 4).
22. **Frontal lobe below antennal toruli.** (0) absent; (1) present (Delvare, 2017: cf. fig. 162).
23. **Orientation of antennal toruli.** (0) lateral and ventral margins of toruli not raised (Delvare, 2017: cf. fig. 38); (1) lateral and ventral margins of toruli raised.
24. **Separation of toruli.** (0) 1–2 times the torular diameter; (1) less than diameter of torulus. (Delvare, 2017: cf. fig. 38).
25. **Interantennal projection from lateral view.** (0) absent, not visible from lateral view or prominent but not discoid; (1) projection prominent and sulcate; (2) projection prominent, discoid, not or hardly sulcate on top (Delvare, 2017: cf. fig. 82).
26. **Antennal scrobes.** (0) present and shallow to moderately deep, never carinately margined;

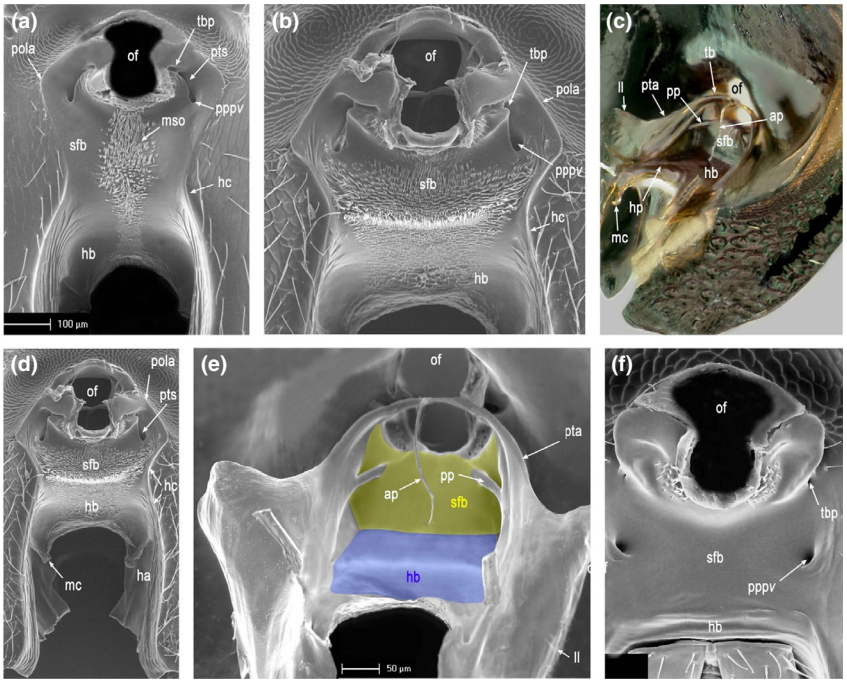

Fig. 4. Tentorial complex for Haltichellinae. (a) *Hockeria bifasciata*; (b–e) *Antrocephalus* sp.; (f) *Notaspidium giganteum*. (a, b, d, f) subforaminal and hypostomal bridges posterior view; (c, e) Tentorium anterolateral view. Abbreviations in Table 2. [Colour figure can be viewed at wileyonlinelibrary.com]

(1) present and deep, mostly carinately margined laterally (Abul-Sood et al., 2018: cf. fig. 2).

27. **Frontal horns.** (0) absent (Delvare, 2017: cf. fig. 11); (1) present (Delvare and Copeland, 2018: cf. figs 31–42).

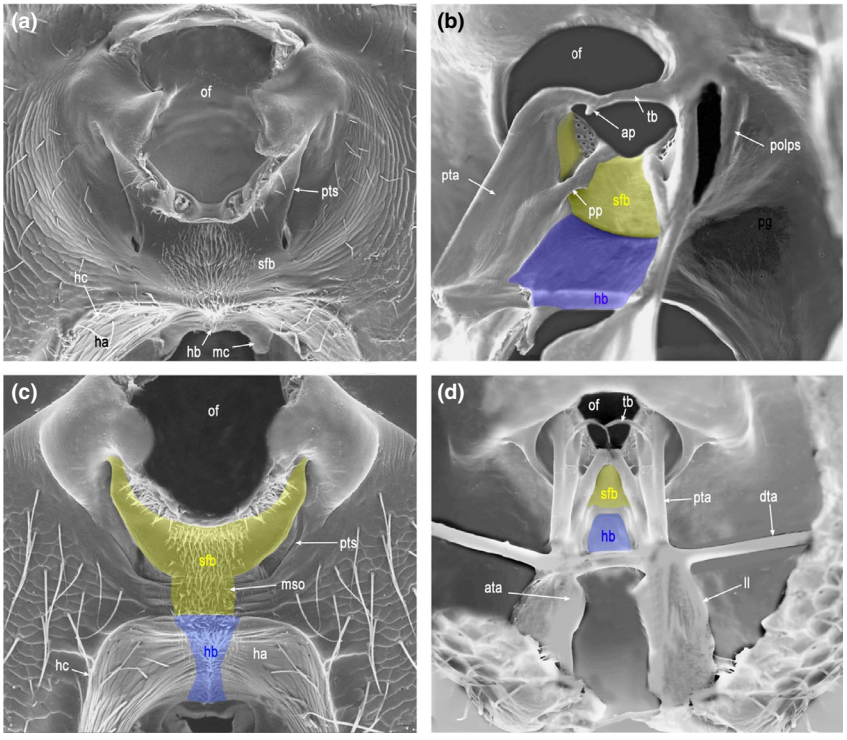

Fig. 5. Tentorial complex for Phasgonophorinae. (a–b) *Trigonura* sp.; (c–d) *Stypiura* sp. (a, c) subforaminal and hypostomal bridges posterior view; (b, d) Tentorium. Abbreviations in Table 2. [Colour figure can be viewed at wileyonlinelibrary.com]

Fig. 6. Tentorial complex for Brachymeriinae. (a–d) *Brachymeria minuta*. (a) Head posterior view; (b) subforaminal and hypostomal bridges posterior view; (c–d) Tentorium anterior and anterolateral views. Abbreviations in Table 2. [Colour figure can be viewed at wileyonlinelibrary.com]

28. **Postoccipital dorsolateral pit for attachment of cervical muscles.** (0) absent (Fig. 4a); (1) present (Fig. 3b).
29. **Postgenal groove.** (0) absent (Fig. 4a); (1) present, not accompanied by postgenal lamina (Figs 3a and 6a).
30. **Posterior tentorial pits/sulci.** (0) present as sulci (Figs 2c, 5c and 7c); (1) absent (Figs 6b, 7a and 8a,e,f); (2) reduced to sulci linking posterior end of posterior tentorial arm (pta) to tentorial bridge pit (tbp) (Fig. 4a,b,d).
31. **Hypostomal bridge (hb). (**0) mostly subforaminal bridge expanded, hypostomal bridge quite reduced or not differentiated (Figs 2a,d and 3b); (1) hypostomal bridge present, distinct from subforaminal bridge (Figs 4b, 5c, 6b–c, 7f and 8b).
32. **Level of subforaminal bridge.** (0) at same level with postgena; (1) sunk down compared to postgena (Fig. 6b); (2) in front of postgenal bridge (Fig. 3e).
33. **Width of hypostomal bridge relative to occipital foramen (of).** (0) narrower than foramen (Figs 2a–b and 3b); (1) at least as broad as foramen (Figs 4b, 5b, 6d, 7e–f and 8b).
34. **Median strip of ornamentation (subforaminal microtrichia sensu Burks and Heraty, 2015) on hypostomal bridge (hb).** (0) present as a set of cuticular ridges or digitiform expansions (Figs 4d, 5a and 6b); (1) absent or virtually so (Figs 4f and 8f).
35. **Width of median strip of ornamentation (mso).** (0) strip narrow, <¼ width of hypostomal bridge (Fig. 3c); (1) strip wider, e.g. ≥1/3 width of hypostomal bridge (Figs 4a–b and 6b).
36. **Shape of hypostomal carina (hc).** (0) forming a complete arch above the hypostomal bridge (Fig. 7a); (1) forming an incomplete arch above the hypostoma and hypostomal bridge (Fig. 3c); (2) extended above and joining the lateral edge postoccipital lateral arm (pola) (Fig. 4a–b).
37. **Maxillary condyles (mc).** (0) close to each other (Figs 2a and 3b); (1) somewhat distant (Fig. 5a); (2) far from each other (Figs 4d, 6b and 7e,g).

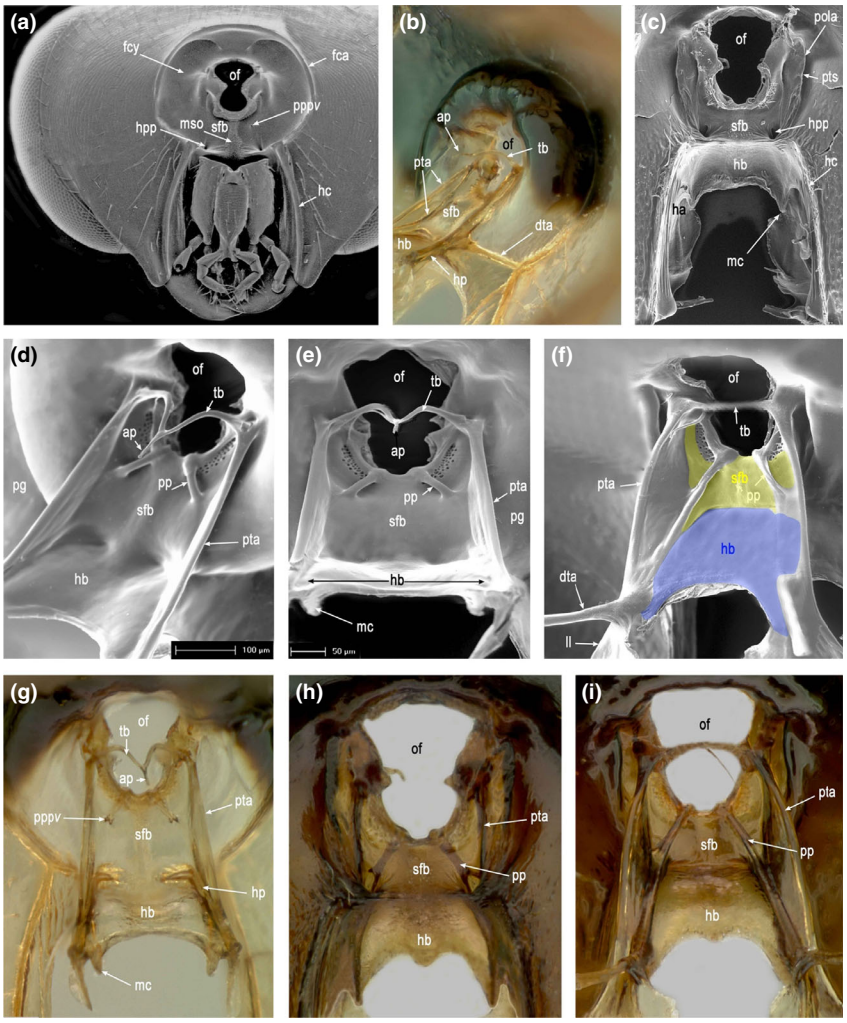

Fig. 7. Tentorial complex for Chalcidinae. (a, b, d, e, g) *Conura decisa*. (c, f, h, i) *Chalcis myrifex*. (a, c, h) subforaminal and hypostomal bridges posterior view; (b, d–g, i) Tentorium anterior and anterolateral views. Abbreviations in Table 2. [Colour figure can be viewed at wileyonlinelibrary.com]

38. **Cardo.** (0) triangular; (1) elongate but with expanded, triangular apex; (2) stick-like; (3) fusiform.
39. **Orientation of hypostoma and hypostomal bridge relative to subforaminal bridge (sfb).** (0) bridges in same plan or hypostomal bridge hardly sloping; (1) bridges forming together an obtuse angle (Figs 4a, 6c and 7f); (2) bridges forming together a right to acute angle (Fig. 8a,c,d,f).
40. **Length of hypostomal bridge.** (0) bridge short or vestigial, much shorter than subforaminal bridge (Figs 2a, and 3c); (1) bridge long to very long, at least as long as subforaminal bridge (Figs 5b, 6c and 7c).
41. **Lateral lamella (ll) on anterior tentorial arm (ata).** (0) narrow; (1) moderately to very broad (Fig. 5d); (2) narrow but with broad apical lobe (Fig. 3d); (3) very broad and continuing on posterior tentorial arm (pta) (Fig. 4c,e).
42. **Structure of posterior tentorial arm (pta).** (0) a sclerotized triangular plate (Fig. 2d); (1) a simple, thick and strongly sclerotized arm (Fig. 6c); (2) including 2 arms, dorsally the pta itself, ventrally a subforaminal process (sfp) along surface of subforaminal bridge (Fig. 7i).
43. **Insertion of dorsal tentorial arm (dta).** (0) evidently above lower eye margin, at least at mid height of eye (Fig. 2e); (1) below, at or slightly above ventral eye margin (Figs 3d and 5d).
44. **ata-pta intersection.** (0) far from base of maxillary condyles (mc) (Fig. 5b); (1) near or at base of base of maxillary condyles (Fig. 7i).
45. **dta-pta intersection.** (0) at ata-pta intersection (Fig. 7b,i); (1) above ata-pta intersection.
46. **Position of ata apex relative to surface of hypostomal bridge.** (0) ata not joining surface of

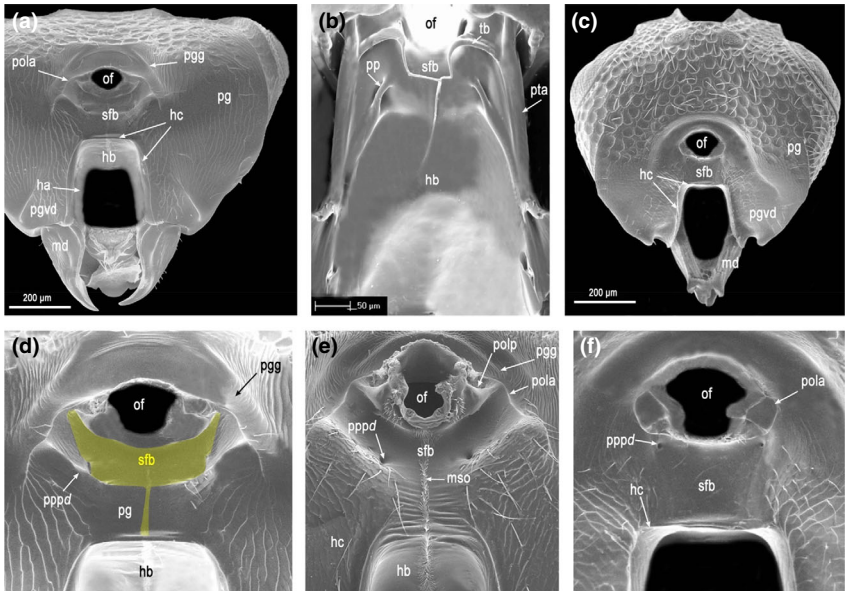

Fig. 8. Tentorial complex for Epitraninae and Dirhininae. (a, d) *Epitranus inops*. (b, e) *Epitranus observator*. (c, f) *Dirhinus anthracia*. (a, c) Head posterior view; (b) Tentorium anterior view; (d–f) subforaminal and hypostomal bridges posterior view. Abbreviations in Table 2. [Colour figure can be viewed at wileyonlinelibrary.com]

hypostomal bridge (Fig. 3d); (1) apical part of ata forming process along lateral edge of hypostomal bridge (Fig. 7i).

47. **Pits at dorsal end of ata.** (0) absent (Fig. 4a,b, d); (1) present (Figs 6b and 7a,c).
48. **Position of dorsal end of posterior process (ppd).** (0) on ventral margin of occipital foramen (of) (Figs 5b, 6c and 7h); (1) below ventral margin of occipital foramen (Fig. 8b).
49. **Pits at dorsal end of posterior process (pppd).** (0) pits absent (Fig. 5c); (1) pits present (Fig. 8e–f).
50. **Position of ventral end of posterior process (ppv).** (0) intercepting pta (Figs 4e and 5b); (1) on surface of subforaminal bridge (Figs 6c and 7f).
51. **Pits at ventral end of posterior process (pppv).** (0) pits absent (Fig. 5c); (1) pits present (Figs 4b, 6b and 7a).
52. **Tentorial bridge (tb).** (0) thick, well-sclerotized and forming a T-like structure with anterior process (AP) (Fig. 2a); (1) thin, slightly sclerotized and forming Y-like structure with ap (Figs 3d, 4e, 5d and 7e).
53. **Postoccipital lateral arm (pola).** (0) visible only on either side of occipital foramen (of) (Fig. 5a,c); (1) joining ventrally the hypostomal carinae (Fig. 4a,b,d).
54. **Number of separate claval segments in female.** (0) three; (1) two; (2) one.
55. **Multiporous plate sensilla (mps) position relative to antennal surface in female.** (0) all mps raised above surface of flagellum (Heraty et al., 2013: cf. fig. 2f); (1) at least some mps sunken (Delvare, 2017: cf. fig. 19).
56. **Number of flagellomeres in male.** (0) 11; (1) nine; (2) seven.
57. **Modified (long or spatulate) hairs on male flagellomeres.** (0) absent; (1) present (Delvare, 2017: cf. fig. 48).
58. **Posterior margin of pronotum.** (0) straight or slightly concave; (1) strongly concave (Gul et al., in press: cf. fig. 10E).
59. **Relative position of tegula and humeral plate.** (0) tegula not covering humeral plate (Delvare, 2017: cf. fig. 39); (1) tegula covering humeral plate (Delvare, 2017: cf. fig. 5).
60. **Tegula position.** (0) anterior corner of tegula abutting against marginal rim of mesoscutum; (1) tegula evidently tapering anteriorly, its anterior corner covered by lateral rim of mesoscutum.
61. **Large setiferous cells on mesoscutum.** (0) absent; (1) present (Delvare, 2017: cf. fig. 13).
62. **Parascutal and axillar carinae.** (0) V-shaped connection or not meeting at transscutal articulation; (1) U-shaped connection over tegula at transscutal articulation (Delvare, 2017: cf. fig. 22).
63. **Axilla, tooth facing projecting anterior inner limit of axillula.** (0) absent; (1) present (Delvare, 2017: cf. fig. 83).
64. **Differentiation of axillula.** (0) axillula absent or not differentiated; (1) axillula present (Delvare, 2017: cf. fig. 22).

65. **Structure of inner margin of axillula.** (0) no evident structure visible; (1) raised carina (Delvare, 2017: cf. fig. 22).
66. **Frenal area of the mesoscutellum.** (0) not marked dorsally (Delvare and Copeland, 2018: cf. fig. 51); (1) defined completely across mesoscutellum.
67. **Frenum orientation.** (0) frenum sloping to vertical (Abul-Sood et al., 2018: cf. fig. 10); (1) frenum reflexed (Delvare, 2017: cf. fig. 22).
68. **Declination of propodeum dorsal surface (lateral view).** (0) sloping relative to longitudinal axis of mesonotum (Gul et al., in press: cf. fig. 4B); (1) flat and in the same plane as mesonotum (Delvare and Copeland, 2018: cf. fig. 148).
69. **Shape of propodeal spiracle.** (0) subcircular to elliptical; (1) slit-like.
70. **Orientation of propodeal spiracle.** (0) oblique; (1) vertical (Delvare, 1992: cf. figs 133–140).
71. **Setose anterolateral areola on propodeum** (horizontal areola between anterior margin of propodeum and spiracle)**.** (0) absent; (1) present (Delvare, 1992: cf. fig. 520).
72. **Posteroventral extension of pronotum.** (0) not extending ventrally across prepectus; (1) with an extension that articulates or crosses the prepectus (Delvare, 1992: cf. fig. 126).
73. **Emargination of pronotum around mesothoracic spiracle.** (0) present, lateral panel emarginate around spiracle (Abul-Sood et al., 2018: cf. fig. 10); (1) absent, lateral panel not emarginate around spiracle; (2) inconspicuous, lateral panel slightly emarginate and bearing dense patch of setae hiding spiracle.
74. **Presence and shape of prosternal discrimen.** (0) visible as a channel, a groove or a ridge; (1) absent.
75. **Prosternum shape.** (0) rounded between ventral and posterior surface or surfaces not distinct; (1) angulate or carinate at the limit between ventral and posterior surface; (2) with vertical lamina at limit between ventral and posterior surface.
76. **Separation between anterior and posterior surface of prosternum.** (0) absent or if present straight line; (1) median process, dentiform or lamelliform.
77. **Profurcal pit.** (0) present; (1) absent.
78. **Lobes on margin of dorsal plate of profurca.** (0) absent; (1) two lobes/projections present.
79. **Ventral plate of profurca.** (0) one surface visible; (1) two surfaces visible, forming a right angle together.
80. **Apical stripe of prosternum.** (0) apparent not sunken within body; (1) internal, sunken within body.
81. **Ornamentation of ventral belt of prepectus.** (0) medioventral areola present only (Delvare, 1992: cf. fig. 126); (1) small and sharp medioventral tooth; (2) large medioventral tooth (Delvare and Copeland, 2018: cf. figs 61–64).
82. **Projection of mesothoracic spiracle.** (0) not projecting, but visible externally (Abul-Sood et al., 2018: cf. fig. 10); (1) hidden externally (Delvare, 2017: cf. fig. 23); (2) partly and hardly visible as hidden by a patch of hairs on posterior margin of pronotum.
83. **Structure of lateral panel of prepectus.** (0) without fovea or raised rim (Abul-Sood et al., 2018: cf. fig. 10); (1) medially foveate, with posterior and/or dorsal rim and small anterodorsal projection (Delvare and Copeland, 2018: cf. figs 62–65).
84. **Size and shape of exposed lateral panel of prepectus.** (0) as tall or taller than long, more than half tegula length; (1) longer than tall, more than half tegula length; (2) small, less than half tegula length (Abul-Sood et al., 2018: cf. fig. 10); (3) lateral panel not apparent.
85. **Prepectus relationship to tegula.** (0) prepectus reaching tegula (Delvare, 2017: cf. fig. 5); (1) prepectus not reaching tegula (Abul-Sood et al., 2018: cf. fig. 10).
86. **Setation of lateral panel of prepectus.** (0) setose (Delvare, 2017: cf. Fig. 5); (1) bare (Abul-Sood et al., 2018: cf. Fig. 10).
87. **Posteroventral margin of prepectus.** (0) ventral margin partially or completely fused medially with episternum; (1) completely separated from mesepisternum.
88. **Mesepisternum: epicnemium.** (0) absent (Delvare, 1992: cf. fig. 482); (1) present, and completely delimited by carina (Abul-Sood et al., 2018: cf. fig. 13).
89. **Mesothoracic discrimen.** (0) sulcate or foveate (Delvare, 1992: cf. fig. 130); (1) raised carina or bump anteriorly, foveate groove posteriorly (Delvare, 2017: cf. fig. 7f); (2) raised carina overall; (3) as anchor-like ornamentation with median carina (Abul-Sood et al., 2018: cf. fig. 13).
90. **Position of mesofurcal pit.** (0) adjacent to mesocoxal cavity; (1) on mesotrochantinal plate.
91. **Shape of metepimeron.** (0) subtriangular (Delvare, 2017: cf. fig. 7); (1) broadly rectangular or squared (Delvare, 2017: cf. fig. 14).
92. **Number of metafurcal pits.** (0) lateral (paired) pits; (1) single median pit (Abul-Sood et al., 2018: cf. fig. 15); (2) pits absent.
93. **Inner lamella of metadiscrimen.** (0) As usual, not especially raised; (1) strongly raised.
94. **Metepisternal ventral shelf.** (0) absent; (1) present above mid coxae, short (Abul-Sood et al.,

2018: cf. fig. 15); (2) present above mid coxae, long.

95. **Submedian teeth at posteroventral edge of metepisternal shelf.** (0) absent; (1) present (Delvare and Copeland, 2018: cf. fig. 12).
96. **Ornamentation between metacoxae.** (0) median groove (Delvare, 2017: cf. fig. 6h); (1) single median carina present (Delvare, 1992: cf. fig. 519); (2) two submedian carinae present, converging posteriorly; (3) two submedian carinae present, parallel and short; (4) absent.
97. **Carina connecting hind coxal and propodeal foramina.** (0) absent; (1) present.
98. **Number of setae on humeral plate.** (0) >four; (1) ≤four.
99. **Basal posterior lobe of forewing.** (0) absent; (1) present (Abul-Sood et al., 2018: cf. fig. 21).
100. **Apicoventral tuft of setae on costal cell.** (0) absent; (1) present (Abul-Sood et al., 2018: cf. fig. 22).
101. **Hyaline break on parastigma.** (0) present (Delvare and Copeland, 2018: cf. fig. 15); (1) absent (Abul-Sood et al., 2018: cf. fig. 63).
102. **Position of marginal vein relatively to front margin of wing.** (0) along margin (Abul-Sood et al., 2018: cf. fig. 63); (1) somewhat removed from margin (Delvare, 2017: cf. fig. 127).
103. **Length of marginal vein of forewing.** (0) 1–3× stigmal vein + stigma length (Abul-Sood et al., 2018: cf. fig. 63); (1) >3× stigmal vein + stigma length (Delvare, 2017: cf. fig. 127); (2) >10× length of stigmal vein plus stigma (Delvare and Copeland, 2018: cf. fig. 90).
104. **Length of postmarginal vein of forewing (fw).** (0) longer than stigmal vein + stigma, shorter than costal cell (Abul-Sood et al., 2018: cf. fig. 63); (1) 1–2× as long as the stigmal vein; (2) absent or shorter than stigmal vein + stigma (Delvare, 2017: cf. fig. 127).
105. **Uncus of stigmal vein of forewing.** (0) present and projecting as a linear process; (1) absent (Delvare, 2017: cf. fig. 127).
106. **Arrangement of uncal sensilla.** (0) arranged in line (Delvare and Copeland, 2018: cf. fig. 89); (1) grouped in a single cluster; (2) two pairs separated by a short space.
107. **Location of basal hamulus.** (0) near the others; (1) distant from the others (Delvare, 2017: cf. fig. 45).
108. **Shape of first hamulus.** (0) curved towards wing surface, like the other hamuli; (1) straight or only slightly curved, with others strongly curved towards wing surface; (Delvare, 2017: cf. fig. 45); (2) curved towards base of hind wing, with others curved towards wing surface.
109. **Line of setation on posterior surface of procoxa.** (0) absent; (1) present (Delvare, 1992: cf. fig. 549).
110. **Apical ornamentation of protibia.** (0) without horizontally directed stout spur or elongation; (1) with horizontally directed socketed spur (Abul-Sood et al., 2018: cf. fig. 17); (2) without socketed spur but distinctly expanded giving the appearance of a spur.
111. **Pegs at apex of mesotibia.** (0) absent; (1) present (Abul-Sood et al., 2018: cf. fig. 18).
112. **Shape of metacoxa.** (0) coxa not enlarged; (1) coxa enlarged and/or elongate (Delvare, 2017: cf. figs 37, 41).
113. **Shape of metafemur.** (0) not enlarged (≥3× as long as broad); (1) enlarged (≤3× as long as broad) (Delvare, 2017: cf. figs 37, 41).
114. **Ventral ornamentation of metafemur.** (0) without denticles or teeth ventrally; (1) with small, uniform teeth similar to blade of a saw over most of length (Delvare and Copeland, 2018: cf. figs 76–82); (2) with large, regular, lobe like teeth (Delvare, 2017: cf. figs 37, 41).
115. **Position of basal tooth of metafemur.** (0) near base of femur (Delvare, 2017: cf. figs 37, 41); (1) at mid-length of femur.
116. **Line of stout bristles on inner surface of metafemur.** (0) absent; (1) present (Delvare, 1992: cf. fig. 149).
117. **Tarsal scrobe on apicodorsal surface of metatibia.** (0) absent or short, never with tooth or protrusion above (Delvare, 2017: cf. fig. 41); (1) present, long, without tooth or protrusion above (Delvare and Copeland, 2018: cf. fig. 84); (2) present, long, with a tooth or protrusion above (Delvare, 2017: cf. fig. 62).
118. **Apex of metatibia, shape.** (0) truncate at right angle (Delvare, 2017: cf. fig. 24); (1) diagonally truncate, posteroventral corner acute (Delvare, 2017: cf. fig. 41); (2) diagonally truncate, posteroventral corner elongated into spine (Delvare, 2017: cf. fig. 56).
119. **Number of apical spurs on metatibia.** (0) two spurs (Delvare, 2017: cf. fig. 24); (1) one spur (Delvare, 2017: cf. fig. 42); (2) no spur (Delvare, 2017: cf. fig. 56).
120. **Ventral carinae of metatibia.** (0) absent; (1) two ventral carinae present, one lateral and one mesal (Delvare, 2017: cf. fig. 89).
121. **Carina on inner surface of metatibia.** (0) absent; (1) present.
122. **Tarsal claws.** (0) simple; (1) pectinate, having 1–2 peg-like extra projection(s) (Delvare, 1992: cf. fig. 554); (2) with basal tooth (Abul-Sood et al., 2018: cf. fig. 20).

123. **Spatulate seta on hind tarsal claw.** (0) absent; (1) present (Delvare, 2017: cf. fig. 43).
124. **Basal lamina on petiole.** (0) absent; (1) present (Delvare, 1992: cf. fig. 176).
125. **Insertion of petiole on propodeum.** (0) at apex near metacoxal foramina (Delvare, 1992: cf. fig. 16); (1) at base of propodeum, near posterior margin of metanotum (Bouček, 1988: cf. fig. 100).
126. **Relationship between petiole and propodeum.** (0) body of petiole entering propodeum (Steffan, 1957: cf. fig. 1); (1) petiole with complete lamina surrounding petiolar foramen of propodeum (Steffan, 1957: cf. figs 4–6); (2) petiole with ventral lamina abutting against petiolar foramen (Steffan, 1957: cf. figs 9–10); (3) condyle only entering propodeum (Steffan, 1957: cf. fig. 11).
127. **Fusion of petiole with first gastral sternite in females.** (0) not fused; (1) fused (Delvare and Copeland, 2018: cf. fig. 108).
128. **Transverse carina in front of cercal plates.** (0) absent; (1) present, cerci inserted in foveae situated just behind the carina (Delvare, 2017: cf. fig. 10e); (2) present, cerci situated posteriorly to carina (Abul-Sood et al., 2018: cf. fig. 24).
129. **Relative placement of hypopygium tip.** (0) in basal half (Abul-Sood et al., 2018: cf. fig. 24); (1) near tip of gaster; (2) somewhat beyond tip of gaster, apex densely setose (Delvare, 1992: cf. figs 204–206).
130. **Orientation of ovipositor sheaths.** (0) straight (Delvare, 2017: cf. fig. 26); (1) curved downwards.

Morphological analyses: analytical workflow

The matrix was analyzed with parsimony (PAUP* v.4.0a; Swofford, 2003). Analyses were first performed with unordered, equally weighted and nonadditive characters. A traditional heuristic search was conducted using 1000 random addition sequences (RAS) to obtain an initial tree and "tree bisection and reconnection (TBR)" as branch swapping option. Ten trees were retained at each step. Robustness of the topology was assessed by bootstrap procedures (100 replicates; TBR RAS 10; one tree retained at each step). Once this unweighted search was completed, we ensured that only the most parsimonious trees were kept in the memory using the "filter trees" option (filtering criteria = best score). All of the equally most parsimonious trees were then used for successive weighting of characters to reduce the weighting of homoplastic characters. Characters were reweighted according to their rescaled consistency index with a base weight of 1. An heuristic search was performed on the reweighted matrix using the same options as for the initial analysis. After this search, characters were reweighted again on the basis of the new trees and this procedure was repeated until a constant length was obtained. Finally, we constrained the set of taxa used for the morphological analysis to fit with each of the three conflicting topologies inferred from the UCE dataset. Character transformations were mapped on the majority-rule consensus tree of the unweighted analysis and the three UCE trees in PAUP* using the ACCTRAN optimization strategy. The morphological matrix, the majority-rule consensus tree of the unweighted analysis of the morphological data and the three UCE trees were included in a nexus file built with Mesquite v.3.31 (Maddison and Maddison, 2018). Reconstruction of ancestral character states was performed with a parsimony approach and consistency index (CI) and retention index (RI) for each character were computed.

Computational resources

Analyses were performed on a Dell PowerEdge T630 server with two 10-core Intel(R) Xeon(R) CPUs E5-2687W v3 @ 3.10GHz and on the Genotoul Cluster (INRA, Toulouse).

Results

UCE dataset

The final UCE dataset (to which we will refer to as the "complete dataset") included 151 taxa (Table S1). No cross-contaminations were detected. In the first round, TreeShrink detected outlier long branches in 155 gene trees. Between one and 12 samples were flagged and removed per gene tree (average = 2 samples; Table S2). In the second round, TreeShrink detected outlier long branches in 28 gene trees. The final matrix (70% complete) included 538 UCEs and taxa were represented by 19 to 528 UCEs (median 478; Table S1). Five taxa had >85% missing UCEs. The alignment contained 283 634 bp, 70.6% of which were parsimony-informative. The percentage of missing data was 20.1%, the percentage of gaps was 16.1% and the GC content was 40.9%. Gap content for taxa (that can either result from the alignment of full length UCEs or capture of partial UCEs) ranged from to 2.2 to 37.0% (median 13.3%).

Phylogenetic inference from the UCE dataset

In the Results section subfamily and tribe names are those of the current classification (Table 1).

PartitionFinder2 used in combination with the SWSC method split the UCE dataset into 890 partitions. ML (Figs S1–S2, Appendix S1), ASTRAL (Fig. S3) and ASTRID (Fig. S4) trees were globally well-resolved. The normalized quartet score of the ASTRAL tree was 0.91, which indicates a high degree of congruence between the species tree and the input gene trees. Regardless of the method used, Chalcididae always was recovered as monophyletic with strong support. Of the six recognized subfamilies (Table 1, current classification), only Chalcidinae was not monophyletic. With the exception of Hybothoracini and Haltichellini, all tribes were monophyletic with high support values. Of the 29 nonmonotypic genera in the dataset, only 16 were recovered monophyletic.

Shallow and intermediate relationships were similar among analytical methods. About 10 unsupported topological conflicts were highlighted. Most of the time, these conflicts involved taxa with a high level of missing UCEs (>85%). Removal of these taxa resulted in topological reconciliation of subtrees in which they were included but did not impact the rest of the trees (Appendix S1). Highly supported conflicts were observed in the deepest nodes of the phylogeny. Although four moderately to highly supported clades were inferred by ML (Fig. 1, topology A), Chalcididae clustered into two highly supported clades in the ASTRAL tree (Haltichellinae vs. all other Chalcididae; Fig. 1, topology B) and three poorly to highly supported clades were inferred by ASTRID (Fig. 1, topology C). Notably, these conflicts were still observed when nodes with BP < 50 were collapsed in individual gene trees before species tree inference by ASTRAL (Fig. S3; normalized quartet score = 0.98). For brevity, we will hereafter refer to the Brachymeriini + Dirhininae + Epitraninae + Phasgonophorini + Smicromorphinae clade (Fig. 1) as the "BDEPS" clade.

Exploration of topological conflicts observed with the UCE dataset

Analysis of bootstrap ML trees showed that topology A was recovered in *c*. 80% of the replicates and topology C was recovered in the remaining 20%. Topology B was recovered when ML trees were midpoint-rooted (Fig. S1C) instead of outgroup-rooted. Visualization of individual UCE trees revealed that ingroups were monophyletic in only 51 of the 538 trees (i.e. 9.48%; Appendix S1). Interestingly, when the set of input trees for the ASTRAL analysis was reduced to these 51 trees, ASTRAL inferred topology C (Fig. S3C). Neither missing data nor gap content appeared phylogenetically clustered on the ML, ASTRAL or ASTRID topologies ($P > 0.05$), which means that taxa with high percentages of missing data/gaps did not cluster together more often than expected by chance. The optimal number of clusters of loci as estimated by the gap statistics on the matrix of geodesic distances among individual gene trees was one (Fig. S5). The GGI approach showed that of the 538 UCEs, 220 (40.9%) supported topology A; 167 (31.0%) supported topology C and 151 (28.1%) supported topology B, with either significant (<0.05) or nonsignificant *P*-values (Fig. 9). Topology A had a significantly best fit for 32 UCEs; topology B had a significantly best fit for six UCEs and topology C had a significantly best fit for one UCE. Therefore, there was a slightly higher support for topology A in the collection of analyzed UCEs but no clear trend toward either topology. Spearman's rank correlation tests showed a significant negative correlation between GC content of the UCEs (Table S3) and the average support of individual gene trees (Fig. S6). There was a higher difference between observed base composition and that predicted under the substitution model for GC-rich UCEs. The alpha parameter of the Gamma distribution was positively correlated with the number of sites informative for the parsimony (i.e. UCEs with more homogeneous rates among sites are more informative) and the average support of individual gene trees (Fig. S6). The LB score heterogeneity (Table S3) was negatively correlated with the number of sites informative for the parsimony and the average support of individual gene trees (Fig. S6).

Hierarchical clustering of taxa based on the heterogeneity of LB scores (Table S4, Fig. S7A) suggested that, with a few exceptions (Zavoyini, Tropimeridini, *Belaspidia*), the diversification dynamics of the Haltichellinae was somehow different compared to other subfamilies. Visual observation of the branch lengths of the ML trees confirmed this pattern (Figs S1–S2). Brachymeriini, Chalcidini, Cratocentrinae, Dirhininae, Epitraninae, Phasgonophorini and Smicromorphinae are supported by more elongated external branches. However, the dendrogram did not show obvious evidence to suggest that the position of Cratocentrinae as sister to the other Chalcididae in the topology A could result from an LBA artefact. In the dendrogram built from GC content (Table S4, Fig. S7B), outgroups were not monophyletic and the Haltichellinae split into two groups. One of the subgroups shared similar properties as a few species of Chalcidini and Phasgonophorini.

Outgroup removal did not result in a shift of position for Cratocentrinae and the GHOST tree that accounts for heterotachous evolution was identical to other ML trees (Appendix S1).

Joint analyses (GGI + UCE properties) revealed that heterogeneities of LB scores were not significantly different among the UCEs that supported either topology (Fig. 9b,c). On the contrary, UCEs supporting topology C (with *P*-values significant or not) had a

Fig. 9. Results of the Gene Genealogy Interrogation (GGI) approach and correlation with Ultra-Conserved Element (UCE) properties. (a) Cumulative number of UCEs supporting each topology. Each of the 538 UCE trees are constrained to fit with topologies (a), (b) and (c) and the approximately unbiased (AU) test is used to estimate which constrained tree shows the best fit (highest *P*-value) with the data. Values above the dashed line indicate that the preferred topology had a significantly better fit than the two alternatives ($P < 0.05$). (b) Left: Comparison of GC content of UCEs that support each topology; Right: comparison of GC content between UCEs that significantly support topology (a) and UCEs that nonsignificantly support topology A or support topologies (b) or (c) either significantly or not. The number of UCEs that support each topology (either significantly or not) is provided on the X-axis (c). Left: Comparison of LB score heterogeneity of UCEs that support each topology; Right: comparison of LB score heterogeneity between UCEs that significantly support topology (a) and UCEs that nonsignificantly support topology (a) or support topologies (b) or (c) either significantly or not. No comparison was made for the six and single UCEs that significantly supported topologies B and C respectively as statistical tests would have been meaningless. [Colour figure can be viewed at wileyonlinelibrary.com]

significantly lower GC content (Fig. 9b). Furthermore, the 32 UCEs that significantly supported topology A had a significantly higher GC content (Fig. 9c).

These results suggest that GC content may bias the results towards topology A. To test this hypothesis, data subsets were constructed by incrementally removing the most biased UCEs and nucleotide sites (Tables 3 and 4). To keep computation time reasonable, ML analyses were performed only with RAxML without partitioning. Indeed, all other approaches/models/software infer the same topology from the complete dataset and are certainly subject to the same bias, if any. Although ASTRAL and ASTRID inferred the same topology whatever the data subset analyzed, RAxML inferred topology C instead of topology A when UCEs with GC content >0.48 (i.e. 28% of the UCEs) were removed from the dataset (Table 3, Appendix S1). However, as already observed with the complete dataset, bootstrap support for the position of Chalcidini never reached 100%. The removal of nucleotide sites with GC >0.57 (i.e. 18.9% of the sites) also induced a shift from topology A to topology C for the ML analyses (Table 4, Appendix S1), although here again, the position of Chalcidini was not supported by 100% bootstrap (BP = 80).

Structure of the tentorium

With the exception of pteromalines, which exhibit an original structure of the tentorium and, therefore, of the back of the head, all other outgroups exhibit the same structure, with little variation (see *Chalcedectus* and *Glyphomerus* in Fig. 2). On the inside of the head capsule, the dorsal tentorial arm (dta) abuts on the upper frons and bears moderately narrow lateral lamellae (ll). The posterior tentorial arm (pta) appears as a triangular, strongly sclerotized plate, standing at a right angle with the surface of the postgena. The posterior process (pp) originates near the base of the pta, along the inner surface of the subforaminal bridge (sfb) and reaches dorsally the ventral margin of the occipital foramen (of). The dorsal edge of the pta continues as the tentorial bridge (tb), here thick and strongly sclerotized, and forms a T-like structure with the anterior process (ap). On the outside of the head capsule, deep posterior tentorial sulci (pts) are well visible, the hypostomal carina (hc) is moderately broken mesally, the maxillary condyles (mc) are separated with a reduced, shortly sloping and narrow hypostomal bridge (hb).

Chalcididae differ in three respects from the structure described above: (i) the dorsal tentorial arm (dta) abuts at a much lower level on the cuticle, hardly above the antennal toruli; (ii) the dta on the whole bears a wider lateral lamella, especially the outer one; (iii) the arms of the tentorial bridge (tb) are thinner and form a Y-like structure with the anterior process (ap).

According to our observations, the cephalic skeleton, the tentorium and the bridges separating the occipital and the oral foramen seemed to have followed two different evolutionary pathways: one in Cratocentrinae and another in all other Chalcididae.

In the Cratocentrinae, the anterior (ata) and posterior tentorial arms (pta) are broad (Fig. 3d) and form a strongly sclerotized strip; the lateral lamella of anterior tentorial arm (ll) is apically very broad (Fig. 3d); the hypostomal carina (hc) is widely broken (Fig. 3c), the maxillary condyles (mc) are narrowly separated and the hypostomal bridge (hb) is vestigial (Fig. 3b). The main difference with all other Chalcididae – which probably represents a unique case within Chalcidoidea – is the presence of two bridges. The subforaminal bridge (sfb) is not visible from outside as is mounted on a base at the surface of the postgena (Fig. 3e), which thus forms a true postgenal bridge. Consequently, none of the external landmarks of the tentorium are visible from outside (Fig. 3a). In the mesal part of the head, the postgena merges progressively into the hypostoma and the postgenal bridge merges into the hypostomal bridge (hb) without any visible limit.

The other Chalcididae differ from the Cratocentrinae by the following character states, that are best illustrated in Phasgonophorini (Fig. 5): (i) posterior tentorial arm (pta) not forming an uniformly sclerotized plate but appearing as a septa, re-enforced by two processes: the true pta continuing as a tentorial bridge (tb) on the dorsal edge (Fig. 5d), and, ventrally, the posterior process (pp) (Fig. 5b); (ii) subforaminal bridge (sfb) forming a right to acute angle with hypostoma (ha) and hypostomal bridge (hb) (Fig. 5b);

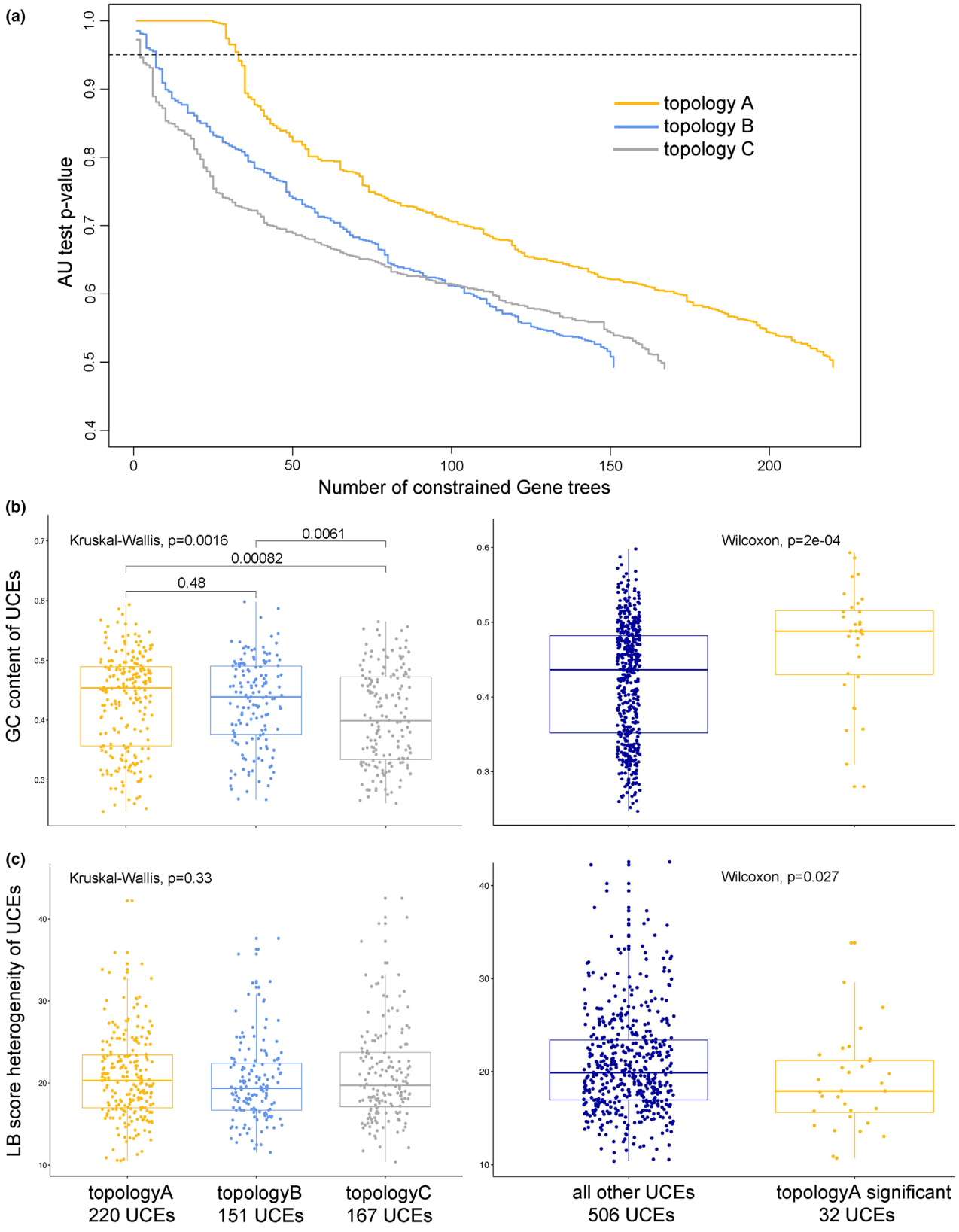

Table 3
Properties of the data subsets analyzed to detect possible systematic bias due to compositional heterogeneity among Ultra-Conserved Elements (UCEs) (GC content) and impact on the branching patterns of the deepest nodes

	GC content threshold to remove UCEs															Complete dataset
	>0.41	>0.42	>0.43	>0.44	>0.45	>0.46	>0.47	>0.48	>0.49	>0.50	>0.51	>0.52	>0.53	>0.54	>0.55	NA
Removed UCEs	318 (59.1%)	310 (57.6%)	286 (53.2%)	265 (49.3%)	240 (44.6%)	214 (39.8%)	182 (33.8%)	152 (28.3%)	120 (22.3%)	88 (16.4%)	69 (12.8%)	45 (8.36%)	33 (6.13%)	22 (4.09%)	15 (2.79%)	(0.00%)
Resulting alignment (bp)	135 091	139 229	151 323	162 104	175 146	187 323	202 875	216 434	230 824	245 194	254 079	264 653	270 267	274 728	277 778	283 634
GC content	0.340	0.342	0.349	0.354	0.361	0.367	0.374	0.380	0.386	0.392	0.396	0.400	0.402	0.405	0.406	0.409
Parsimony informative sites	0.700	0.701	0.703	0.705	0.706	0.707	0.708	0.709	0.709	0.710	0.710	0.710	0.710	0.709	0.709	0.706
Gap content	0.162	0.162	0.161	0.162	0.161	0.162	0.162	0.162	0.162	0.162	0.162	0.161	0.162	0.162	0.162	0.161
Missing data	0.180	0.181	0.184	0.185	0.187	0.189	0.192	0.194	0.196	0.198	0.198	0.199	0.200	0.200	0.201	0.201
Inferred Topology RAxML	C	C	C	C	C	C	C	C	A	A	A	A	A	A	A	A
Inferred Topology ASTRAL	B	B	B	B	B	B	B	B	B	B	B	B	B	B	B	B
Inferred Topology ASTRID	C	C	C	C	C	C	C	C	C	C	C	C	C	C	C	C

Table 4
Properties of the data subsets analyzed to detect possible systematic bias due to compositional heterogeneity among nucleotide sites (GC content) and impact on the branching patterns of the deepest nodes

	GC content threshold to remove nucleotide sites														Complete dataset
	>0.50	>0.51	>0.52	>0.53	>0.54	>0.55	>0.56	>0.57	>0.58	>0.59	>0.60	>0.70	>0.80	>0.90	NA
Removed sites	63 436 (22.4%)	61 440 (21.7%)	60 471 (21.3%)	58 711 (20.7%)	57 820 (20.4%)	56 062 (19.8%)	55 227 (19.5%)	53 551 (18.9%)	52 713 (18.6%)	51 063 (18.0%)	50 242 (17.7%)	37 791 (13.3%)	14 040 (5.00%)	221 (0.08%)	0
Resulting alignment (bp)	220 198	222 194	223 163	224 923	225 814	227 572	228 407	230 083	230 921	232 571	233 392	245 843	269 594	283 413	283 634
Inferred Topology RAxML	C	C	C	C	C	C	C	C	A	A	A	A	A	A	A

(iii) maxillary condyles (mc) more distant from each other (Fig. 5a); (iv) hypostomal bridge (hb) deeply sloping and longer than wide (Fig. 5c); (v) laterally, on either side of the hb, anterior tentorial arm (ata) extending into an hypostomal process (hp), visible from the outside as the hypostomal process pit (hpp) (Fig. 7g–i); (vi) narrow posterior tentorial sulcus (pts) visible, converging ventrally (Fig. 5c); (vii) postoccipital lateral arms (pola) short (Fig. 4a), not extending to ventral end of pts, and strongly converging ventrally.

Phylogenetic analysis of morphological data

The nexus-formatted matrix of morphological characters is available is Appendix S2. Parsimony analysis of the 130 morphological characters with PAUP* produced 1437 equally parsimonious trees (length = 331, CI = 0.544, RI = 0.839, rescaled consistency index (RC) = 0.456) distributed on 13 islands. One island was found in 98% of the searches and consisted in 1421 trees. Other islands were found in 1, 2 or 4% of the searches. The majority-rule consensus tree annotated with the current classification is presented in Fig. S8A. ML and Bayesian analyses recovered Cratocentrinae as sister to Phasgonophorini with moderate support (Fig. S8). Otherwise, the ML, Bayesian and parsimony topologies were similar. Unsurprisingly, bootstrap support for nodes of the morphological trees was poor as compared to the UCE trees. In a similar way to UCEs, morphological data support the monophyly of the family, the monophyly of all subfamilies except Chalcidinae, and the polyphyly of the tribes Haltichellini and Hybothoracini. By contrast with UCE trees, *Zavoya* was recovered as sister to *Notaspidium* with high support and Dirhininae + Epitraninae formed a strongly supported clade. Three rounds of successive weighting were performed to reach a constant length of trees. Fourteen trees were retained (CI = 0.714, RI = 0.907, RC = 0.648, unweighted length = 332), the strict consensus of which is presented in Fig. S8B. In this weighted consensus tree, Smicromorphinae was recovered as sister to the other Chalcididae, which is certainly due to the numerous apomorphies that defined this highly transformed parasitoid. The genus *Conura* was not monophyletic and *Belaspidia* instead of *Tropimeris* was sister to other Haltichellinae. Unweighted and weighted trees were otherwise similar. Weighted trees being longer than unweighted trees they were not retained for future analysis. Figure 10 shows the majority-rule consensus of the 1437 MP trees (unweighted analysis), on which character transformations were mapped with PAUP* using the ACCTRAN optimization strategy (note that Fig. 10 is annotated with the new classification proposed in this study, as this new classification will be used in the Discussion section after formal changes are made). Appendix S3 describes character transformations inferred with PAUP* on the four competing topologies (topologies A,B,C for UCEs and unweighted majority-rule consensus morphological tree; the new classification is used to annotate the excel sheet). Appendix S2 provides the ancestral state reconstruction (parsimony) for each character on the four competing topologies. Appendices S2 and S3 are used in the next section to discuss morphological support of alternative placement of key taxa.

Discussion

The power of UCEs to resolve the tree of life of poorly known groups

So far, UCEs have been used successfully to infer the phylogenies of a few groups of large to medium-sized insects (bees, wasps, ants and weevils: Blaimer et al., 2015, 2016b; Jesovnik et al., 2017; Prebus, 2017; Van Dam et al., 2017; Branstetter et al., 2017a; Bossert et al., 2019). Here, we highlight the power of UCEs for the exploration of hyperdiverse and poorly known groups of small to medium-sized chalcidoid wasps.

We were able to successfully use the universal Hymenoptera probe set designed by Faircloth et al. (2015) (myBaits UCE Hymenoptera 1.5Kv1) to capture UCEs from chalcidoid wasps without any optimization. This confirms the generic nature of UCEs (Bossert and Danforth, 2018).

Three situations can be distinguished in our study that may be encountered in other groups. First, when morphology is informative enough to circumscribe taxa and establish relationships, UCEs and morphology converge to the same results. Second, when morphology is not informative enough or misleading, UCEs are helpful to circumscribe taxa (e.g. genera or tribes) and clarify relationships within taxa. Additional studies of the morphology can then be performed and help discern characters that support the taxa. In summary, UCEs help to enable attainment of resolution between ancestry, convergent evolution or divergent evolution. We confirm that UCEs can be captured from museum specimens (McCormack et al., 2016; Blaimer et al., 2016b), which is a key requirement when working on poorly known/rare groups, as sequencing of type specimens is often required to fix species names. Finally, when neither morphology nor molecules are informative enough to resolve relationships, a systematic exploration of bias as well as the use of different analytical methods and a careful feedback assessment with morphological features is required.

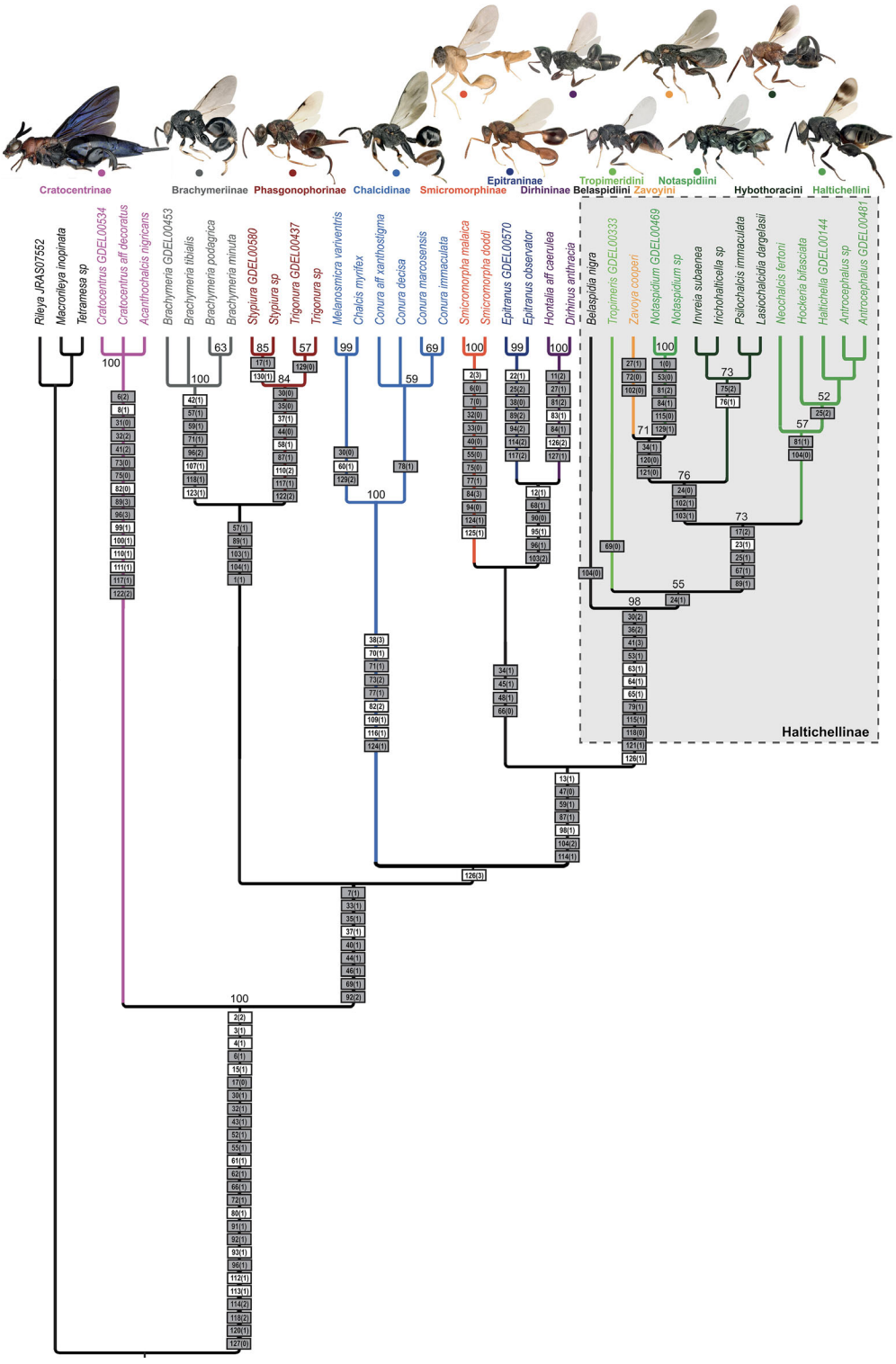

Fig. 10. Results of the morphological analysis. Majority-rule consensus of the 1437 equally parsimonious trees obtained with PAUP* (unweighted analysis). The new classification proposed in this paper and associated colour coding is used to annotate the tree. The same tree also is available in Fig. S8A with the current classification. Bootstrap supports (>50) are depicted at nodes (100 replicates). Character transformations were mapped on tree using the ACCTRAN optimization strategy implemented in PAUP*. White boxes indicate unambiguous transformations (double arrows in PAUP*) of nonhomoplastic characters (CI = 1.00). Grey boxes indicate ambiguous transformations (single arrows in PAUP*) of nonhomoplastic characters (CI = 1.00) or ambiguous (single arrows in PAUP*) and nonambiguous transformations (double arrows in PAUP*) of homoplastic characters (0.50 ≦ CI < 1.00). [Colour figure can be viewed at wileyonlinelibrary.com]

A monophyletic Chalcididae

Inference of character transformations (Appendix S3) and ancestral state reconstructions (Appendix S2) show that Chalcididae can be defined based on 23 apomorphies among which eight are homoplastic (italics): Head and mesosoma strongly sclerotized, punctured and/or areolate distinctly sclerotized not collapsing when dry (character 2, state 2); labrum exposed and abutting anterior to clypeal margin (3,1); labrum plate-like (4,1); *upper margin of clypeus step-like (14,2)*; lateral clypeal sulcus absent (15,1); *clypeus more than three times as broad as long (16,1)*; *cardo stick-like (38,2); posterior tentorial arm as a septa re-enforced with 2 sclerotized processes (42,2); insertion of dorsal tentorial arm about at level with ventral eye margin (43,1);* tentorial bridge thin and forming a Y-like structure with the anterior process (52,1); *multiporous plate sensilla (mps) sunken (55,1)*; presence of large setiferous cells on mesoscutum (61,1); parascutal and axillar carinae with U-shaped connection over tegula at transscutal articulation (62,1); *frenal area of the mesoscutellum completely defined (66,1)*; pronotum with posteroventral extension that articulates or crosses the prepectus (72,1); apical strip of prosternum sunken within body (80,1); *mesepisternum epicnemium present (88,1)*; metepimeron broadly rectangular or square (91,1); inner lamella of metadiscrimen strongly raised (93,1); *metacoxa enlarged and/or elongate (112,1)*; *metafemur enlarged (113,1)*; metatibia with two ventral carinae (120,1); petiole entirely sclerotized but not fused with first gastral sternite (127,0).

A new higher classification for the Chalcididae

Based on our results, we propose a revised higher classification (subfamilies and tribes) for the family (Table 1; Figs 10 and 11). The within-tribe classification was not the purpose of this study and will be reviewed elsewhere. To be conservative, we propose to keep subfamilies in their historical taxonomic rank, but to raise the tribes Phasgonophorini and Brachymeriini to subfamily rank. Within Haltichellinae, we recognize six major monophyletic groups that should be considered as tribes: Belaspidiini (**trib.n.**), Haltichellini, Hybothoracini, Notaspidiini (**trib.n.**), Tropimeridini and Zavoyini. Additionally, the subfamily Phasgonophorinae should include two tribes, Phasgonophorini (**stat.r.**) and Stypiurini (**trib.n.**), to denote the corresponding sister monophyletic groups.

From here onwards, subfamily and tribe names used in text refer to the new classification proposed in this paper (Table 1). In the paragraph below, the term "apomorphies" refers to derived character states that support monophyly of the different groups. Apomorphies that are shared with a few other groups are italicized. A description of the endocephalic structures and their external landmarks observed in the different groups and that are new to this study is presented in Table 5.

*Brachymeriinae (**stat.r.**)*. Examination of the type species of all genera of Brachymeriinae indicates that only *Brachymeria* should be retained as valid. Brachymeriinae is supported by seven apomorphies: posterior tentorial arm a simple, thick and strongly sclerotized process (42,1); male flagellomeres with modified hairs on the underside (57,1); metepisternum with two submedian carinae, converging posteriorly between metacoxa (96,2); first hamulus distant from the others (107,1); apex of metatibia is diagonally truncate, posteroventral corner acute (118,1); hind tarsal claw with special spatulate seta (123,1). Two characters are either shared with Chalcidinae: *propodeum with setose anterolateral areola (71,1)* or with Stypiurini: *hypopygium tip close to tip of gaster (129,1)*.

Chalcidinae. The monophyly of this subfamily in its new circumscription (represented in our study only by specimens belonging to Chalcidini) is sustained by six apomorphies: cardo fusiform (38,3); propodeum with spiracle in vertical orientation (70,1); emargination of pronotum around mesothoracic spiracle inconspicuous and bearing dense patch of setae hiding spiracle (73,2) (however, this character is polymorphic in *Conura*); mesothoracic spiracle partly and hardly visible as hidden by a patch of hairs on posterior margin of pronotum (82,2); procoxa with line of setation on posterior surface (109,1); metafemur with line of stout bristles on inner surface (116,1); and three homoplastic character states: *propodeum with setose anterolateral areola (71,1); profurcal pit absent (77,1); petiole with basal lamina (124,1)*. *Hovachalcis* Steffan, a key Chalcidinae taxon is not included in our analysis as only one specimen (the holotype) is known and it could not be dissected, but it shares several character states with Chalcidinae (e.g. 70,1 and 124,1). We must note that *Hovachalcis* may deserve a tribal status of its own.

Cratocentrinae. The subfamily is supported by 19 apomorphies, five of which are homoplastic (italics): mouth margin thickened and incised for reception of dorsal corner of mandible, mandibular based exposed (6,2); incision on outer surface of mandible (8,1); *two teeth on the right mandible (10,1); anterior tentorial pits not visible externally (18,1);* subforaminal bridge in front of postgenal bridge, not visible from outside (32,2); lateral lamella on anterior tentorial arm narrow but with broad apical lobe (41,2); pronotum with

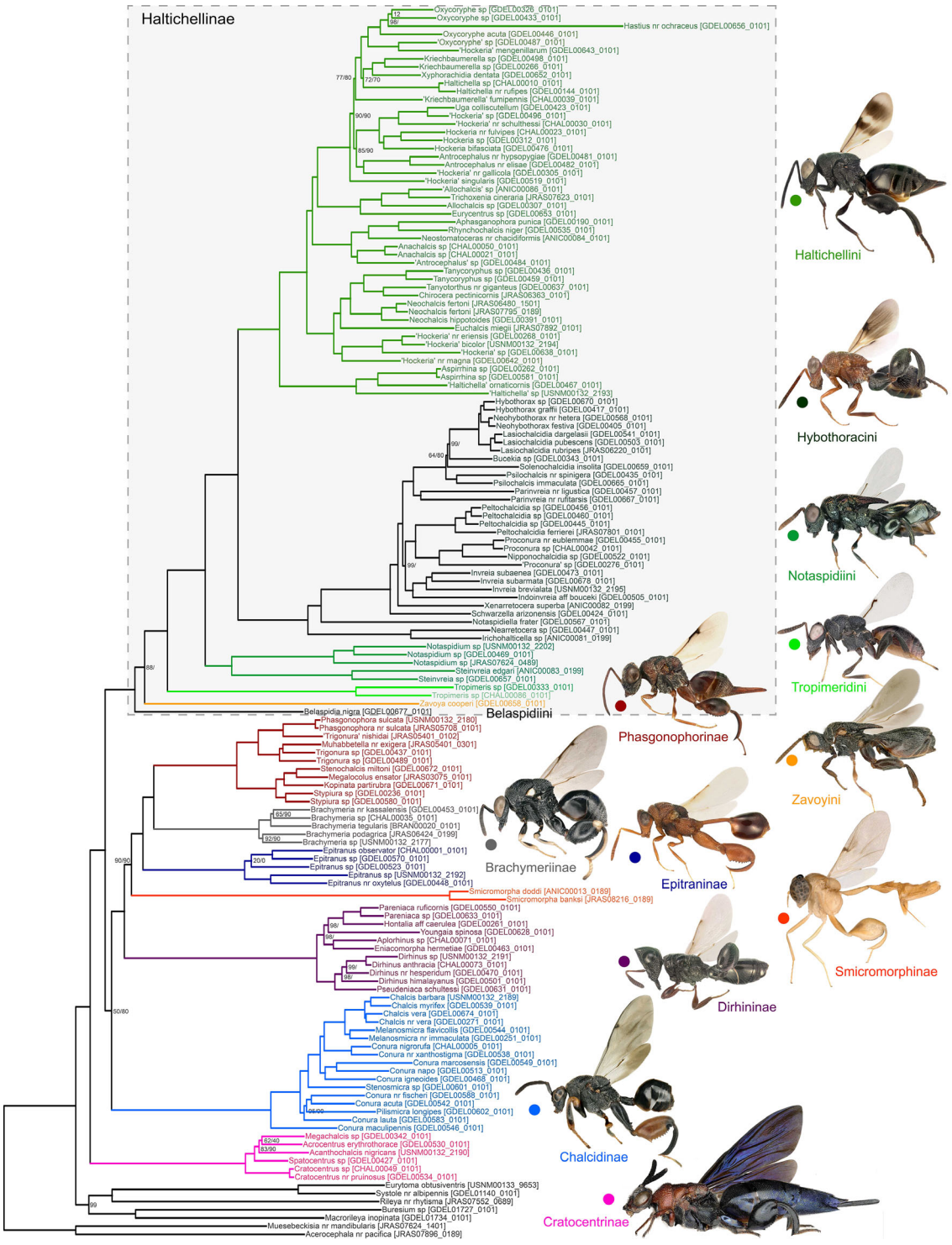

Fig. 11. Preferred topology (UCE topology C) showing the new higher classification of the Chalcididae. The new classification proposed in this paper is used to annotate the tree. Colour coding is similar to Fig. 10. The RAxML tree inferred from the less biased UCEs (GC content ≦ 0.48) is used as a template and bootstrap support values less than 100 are reported at nodes as follows: RAxML on less biased UCEs/RAxML on less biased nucleotides (i.e. with GC content ≦ 0.57). This topology received the highest support from our morphological analysis regarding the position of Cratocentrinae and Chalcidinae. The new classification proposed in this paper is used to annotate the tree. Colour coding is similar to Fig. 3. Within tribe classification including synonymy of invalid genera was not the purpose of this study and will be reviewed elsewhere. Single quotes indicate new genera awaiting description, the genus name used in the annotation is the one obtained when using current identification keys. [Colour figure can be viewed at wileyonlinelibrary.com]

Table 5
Description of cephalic skeleton, tentorium and bridges for all subfamilies of Chalcididae

Characters	Cratocentrinae Fig. 3	Haltichellinae Fig. 4	Phasgonophorinae **stat.r.** Fig. 5	Brachymeriinae **stat.r.** Fig. 6	Chalcidinae Fig. 7	Smicromorphinae	Epitraninae Fig. 8	Dirhininae Fig. 8
anterior tentorial arm (ata)	broad, form a strongly sclerotized strip with pta	not broad, appearing as a septa	not broad, appearing as a septa	not broad, appearing as a septa	not broad, appearing as a septa	not broad, appearing as a septa	not broad, appearing as a septa	not broad, appearing as a septa
hypostomal process pit (hpp)	not visible externally	not visible externally	visible externally	visible at latero-ventral angle of subforaminal bridge (sfb)	visible externally	not visible externally	not visible externally	not visible externally
posterior process (pp)	reaching posterior tentorial arm (pta), reaching the edge of the occipital foramen (of)	reaching pta, reaching the edge of the occipital foramen (of)	reaching pta, reaching the edge of the occipital foramen (of)	ventral apex not reaching pta, but reaching the edge of the occipital foramen (of) dorsally	reaching the edge of the occipital foramen (of) dorsally, reaching pta (*Chalcis* & *Melanosmicra*) or not joining pta (*Conura*) ventrally	n.a.	reaching pta ventrally, but inserted below ventral margin of the of dorsally	reaching pta ventrally, but inserted below ventral margin of the of dorsally
posterior tentorial arm (pta)	broad, form a strongly sclerotized strip with ata	well-sclerotized and appearing as a septa, dorsally continuing as the tb and ventrally joining the pp	well-sclerotized and appearing as a septa, dorsally continuing as the tb and ventrally as the pp	thick and strongly sclerotized, forming an acute angle with the surface of the postgena	not sclerotized but appearing as a septa, with dorsally the true pta continuing as the tb and ventrally joining the pp	n.a.	well-sclerotized and appearing as a septa, continuing dorsally as the tb and ventrally joining the pp	well-sclerotized but appearing as a septa, continuing dorsally as the tb and ventrally joining the pp
pit at dorsal end of posterior process (ppp*d*)	absent	absent	absent	absent	absent	n.a.	present	present
pit at ventral end of posterior process (ppp*v*)	absent	present	absent	present	absent in *Chalcis* and *Melanosmicra*, present in *Conura*	n.a.	absent	absent
posterior tentorial pit (ptp)	absent: pta do not reach the postgena because of the presence of a true postgenal bridge in addition to the subforaminal bridge	appearing as short sulci diverging ventrally and linking the tbp dorsally to the ppp*v* ventrally (except in *Notaspidium* where the sulci are absent)	present as narrow sulci, converging ventrally	completely absent	present as very superficial sulci in *Chalcis*, absent in *Conura*	completely absent	completely absent	completely absent
tentorial bridge pit (tbp)	not visible	visible	not visible	visible	not visible	not visible	not visible	not visible
pits at dorsal end of anterior tentorial arm (ata)	absent	absent	present	present	present	absent	absent	absent

Table 5
(Continued)

Characters	Cratocentrinae Fig. 3	Haltichellinae Fig. 4	Phasgonophorinae **stat.r.** Fig. 5	Brachymeriinae **stat.r.** Fig. 6	Chalcidinae Fig. 7	Smicromorphinae	Epitraninae Fig. 8	Dirhininae Fig. 8
lateral lamella (ll) of anterior tentorial arm (ata)	narrow with broad apical lobes	extending on posterior tentorial arm (pta)	moderately to very broad		moderately to very broad	n.a.	moderately to very broad	moderately to very broad
hypostomal carina (hc)	forming an incomplete arch, widely broken	complete, extended above and joining the pola, except in *Notaspidium*	forming a complete arch	forming an incomplete arch	mainly forms an incomplete arch	forming an incomplete arch	forming a complete arch	forming a complete arch
postoccipital lateral arm (pola)	visible on either side of the of	long, joining ventrally the hypostoma except in *Notaspidium*	short, visible on side of, not extending to ventral end of pts, and converging ventrally	visible on side of the of, parallel to each other and smoothly continuing to the hpp ventrally	visible on side of the of	n.a.	visible on side of the of, diverging from each other	visible on side of the of
maxillary condyles	narrowly separated	widely separated	distant from each other	widely separated	widely separated	n.a.	widely separated	widely separated
hypostomal bridge (hb)	vestigial	distinct, broad and sloping from sfb without limit between them	distinct, deeply sloping and longer than wide	distinct, long	distinct, long	distinct, short	distinct, long	distinct, long
subforaminal bridge (sfb)	in front of pb, mounted on a base on postgena surface, merges into the hypostomal bridge (hb) without any visible limit	sunk down compare to postgena), forming an obtuse angle with hb, or a right to acute angle in *Antrocephalus*, *Zavoya* and *Notaspidium*	sunk down compare to postgena, forming a right to acute angle with hypostoma (ha) and hypostomal bridge (hb	sunk down compare to postgena, without carina between the bridges that form an obtuse angle	sunk down compare to postgena, form an obtuse angle with hb	at the same level as postgena, and in the same plane as hb	sunk down compare to postgena, long, forming an acute angle with hb	sunk down compare to postgena), forming an acute angle with hb
postgenal groove	present	absent	present	generally present	absent	absent	present	absent
median strip of ornamentation (mso)	present, narrow	present and wide, absent in *Notaspidium* and *Zavoya*	present, narrow	present, broad especially on hypostomal process	present, broad especially on hypostomal process	absent	absent, vestigial	

Subfamily names refer to the new classification proposed in this manuscript.

emargination around mesothoracic spiracle (73,0); mesothoracic spiracle visible externally (82,0); *prepectus not reaching tegula (85,1)*; mesothoracic discrimen as anchor-like ornamentation with median carina (89,3); only a single, median metafurcal pit (92,1); metepisternum with two submedian carinae, parallel and short between metacoxae (96,3); forewing with posterobasal lobe (99,1); costal cell with apicoventral tuft of setae (100,1); protibia with horizontally directed socketed spur (110,1); mesotibia with pegs at apex (111,1); *apical spur on metatibia absent (119,2); tarsal claws with basal tooth (122, 2)*; transverse carina in front of cercal plate present with cerci situated posteriorly to carina (128,2). Nevertheless, (73,0) and (82,0) are ambiguous as the groundplan condition for Chalcididae is unknown. Indeed, the mesothoracic spiracle is hidden in Eurytomidae, the putative sister group of Chalcididae. Thus, a hidden mesothoracic spiracle could represent a synapomorphy for the two families and, in this case, the exposed spiracle of the Cratocentrinae should be considered as a reversal. Conversely, a hidden mesothoracic spiracle could be homoplastic.

Haltichellinae. The subfamily is diagnosed by 10 apomorphies, two of which also occur in *Smicromorpha* (italics): posterior tentorial sulci short, only linking the posterior process pit to the tentorial, bridge pit (30,2); hypostomal carina extended above and joining the postoccipital lateral arm (36,2); postoccipital lateral arm joining ventrally the hypostomal carina (53,1); axilla with projecting tooth facing the raised base of axillula (63,1); axillula present and completely delimited (64,1); inner margin of axillula as raised carina (65,1); *mesofurcal pit on mesotrochantinal plate (90,1)*; *median groove between metacoxal foramina (96,0);* inner side of metatibia with carina (121,1); petiole with complete lamina surrounding ventrally the petiolar foramen of the propodeum (126,1).

- ***Belaspidiini (trib.n.)*** is diagnosed by a single apomorphy: delimitation of upper margin of clypeus visible through change in sculpture (14,1). The presence of a posteromedian projection on the mesoscutellum may also define the tribe.
- ***Haltichellini*** is supported by only one apomorphy: the ornamentation of the ventral belt of the prepectus, bearing a sharp medioventral tooth (81,1). Two homoplastic character states are shared with Tropimeridiini: *toruli separated by less than their own diameter (24,1)*; or with Epitraninae: *strongly prominent, mostly not sulcate, interantennal projection (25,2)* (absent in *Neochalcis*).
- ***Hybothoracini*** in its new circumscription is supported by the following apomorphies: prosternum with vertical lamina at limit between the ventral and the posterior surfaces (75,2); presence of median process (dentiform or lamelliform) between anterior and posterior surfaces of prosternum (76,1).
- ***Notaspidiini* (trib.n.)** is diagnosed morphologically by two apomorphies that also are shared by a few other clades: *ventral belt of prepectus with acute median tooth (81,2); lateral panel of prepectus longer than tall (84,1)*. The tribe also contains *Steinvreia* Bouček, which only was present in our molecular analysis as just a few specimens were available and could not be dissected.
- ***Tropimeridini*** is weakly diagnosed by one character state, that is a reversal: propodeum with a circular spiracle, its rim being partly hidden by a lobe formed by the anterior end of the sublateral propodeal carina (69,0).
- ***Zavoyini***, which includes the single genus *Zavoya* Bouček, is supported only by two character states: *presence of frontal horns (27,1),* which also is observed in Dirhininae but may be nonhomologous; posteroventral extension of pronotum not extending ventrally across prepectus (72,0), but this represents a reversal toward the ancestral condition.

Dirhininae. The monophyly of this subfamily has never been contested and is supported by the following apomorphies: lateral panel of prepectus medially foveate (83,1); petiole with ventral lamina abutting against petiolar foramen (126,2); petiole fused with first gastral sternite in female (127,1). The last character state is a reversal toward the ancestral condition. Furthermore, other character states may contribute to define Dirhininae but are homoplastic: *ventral (= inner) tooth of mandibles much shorter than dorsal one (11,2); head with frontal horns (27,1)* (but see Zavoyini); *ventral belt of prepectus with large medioventral tooth (81,2); lateral panel of prepectus longer than tall (84,2)*. In addition, the propodeum has a peculiar ornamentation including an anteromedian areola and the spiracle is placed on the bottom of a setose depression.

Epitraninae. The subfamily comprises only the genus *Epitranus* Walker, and its monophyly has never been questioned. It is unambiguously supported by the following character states: head with frontal lobe below antennal toruli (22,1); cardo triangular (38,0); mesothoracic discrimen as raised carina overall (89,2); metepisternal ventral shelf quite long (94,2); metatibia with long tarsal scrobe on apicodorsal surface, with a tooth or protrusion above (117,2). Additionally, the gaster is strongly bulging ventrally and the antennal scrobes are shallow and often delimited laterally by faint carinae.

Phasgonophorinae (***stat.r.***). The subfamily is well defined by three apomorphies: maxillary condyles somewhat distant from each other (37,1); posterior margin of pronotum strongly concave (58,1); protibia without socketed spur but distinctly expanded giving the appearance of a spur (110,2); and two homoplastic character states within Chalcididae: *posterior tentorial sulci present (30,0); tarsal claws with basal tooth (122,2)*.

- ***Phasgonophorini*** is diagnosed only by a single homoplastic character state (also retrieved in Cratocentrinae): *absence of apical spur on metatibia (119,2)*.
- ***Stypiurini*** **(trib.n.)** is diagnosed by a uniquely derived character state in Chalcididae: ovipositor sheaths curved downward (130,1).

Smicromorphinae. The subfamily is defined by three uniquely derived apomorphies: gaster weakly sclerotized, collapsing when dried (2,3); hypostomal and subforaminal bridges in the same plane (39,0); petiole inserted at base of propodeum (125,1). Several other characters are reversals towards the ancestral condition or homoplastic within Chalcididae but also can be used to define Smicromorphinae: *mandibular base dorsally concealed by genal margin (6,0); mouth margin above mandible not incised for reception of mandible (7,0); subforaminal bridge at same level with postgena (32,0), hypostomal bridge narrower than occipital foramen (33,0); hypostomal bridge short or vestigial, much shorter than subforaminal bridge (40,0); mps raised above surface of flagellum (55,0); prosternum rounded between ventral and posterior surfaces or surfaces not distinct (75,0); lateral panel of prepectus not apparent (84,3); metepisternal ventral shelf absent (94,0); petiole with basal lamina (124,1)*.

Diagnoses of subfamilies and tribes are given in Appendix S4.

Resolving conflicts among methodological approaches

Although there is generally good agreement between morphology and molecules, on the one hand, and between the different UCE analytical approaches, on the other, there are a few conflicts that we discuss below.

Taxa with a high level of missing UCEs. There are unsupported conflicts between concatenation and gene tree reconciliation approaches for the position of taxa with a high level of missing UCEs (>85%: *Hastius* Schmitz, *Solenochalcidia* Steffan, *Pseudeniaca* Masi). The impact of missing data on phylogenetic inference has been widely discussed but no consensus has been reached. Missing data are either considered as deleterious (Lemmon et al., 2009) or not problematic if sufficient informative characters are available to infer relationships (Wiens, 2003; Wiens and Morrill, 2011; Hosner et al., 2016; Streicher et al., 2016). Gene tree reconciliation approaches have been proven robust enough to a high, global level, of missing data (Nute et al., 2018). However, according to our knowledge of their morphology, the position of taxa with a high level of missing data is more accurate in the concatenation approach than in the gene tree reconciliation approaches.

Position of Cratocentrinae. Cratocentrinae is recovered either as sister to all other Chalcididae (ML + ASTRID + Morphology but with weak support) or nested within Chalcididae (ASTRAL; Fig. 1). Spearman correlation tests suggest that evolutionary rate heterogeneity among taxa and nucleotide sites as well as compositional heterogeneity among UCEs could bias the analyses (Fig. S6). Thus, the first hypothesis we explored was that the position of Cratocentrinae as sister to all other Chalcididae in the ML tree resulted from an LBA artefact. Indeed, supermatrix approaches are more sensitive to LBA which, in addition, tend to be reinforced as more and more markers are considered (Boussau et al., 2014). However, hierarchical clustering of taxa properties (Fig. S7), analysis with complex models that considers heterotachous evolution (GHOST; Appendix S1), outgroup removal analysis (Appendix S1) and the nonsignificant difference of scores of LB heterogeneity among UCEs that support topology A and other UCEs (Fig. 9), show that LBA should be excluded. Sampling used in this study could certainly be improved but is representative of the group. More importantly, the outgroups used for this study are the closest relatives to the ingroups (in prep.; see the Methods section).

As described in the results, the cephalic skeleton, the tentorium and the bridges separating the occipital and the oral foramen are structurally different in Cratocentrinae as compared to all other Chalcididae. Besides, the position of Cratocentrinae as sister to all other Chalcididae is supported by nine characters for which Cratocentrinae exhibits the plesiomorphic character state compared to all other Chalcididae. The mouth margin is not incised for reception of mandible (7,0) in Cratocentrinae, whereas it is incised (7,1) in all other Chalcididae but Smicromorphinae. The hypostomal bridge is reduced and not differentiated from subforaminal bridge (31,0), whereas it is distinct from subforaminal bridge (31,1) in the rest of the family. The hypostomal bridge is narrower than the occipital foramen (33,0), whereas it is at least as broad as occipital foramen (33,1) in other Chalcididae but Smicromorphinae. The width of median strip of ornamentation (mso) is narrow (<¼ of the width of hypostomal

bridge) (35,0) whereas it is wide (>1/3 of the width of hb) (35,1) in other Chalcididae, yet the plesiomorphic state also occurs in Phasgonophorinae. The maxillary condyles are close to each other (37,0), whereas they are distant from each other in the rest of the family (37,1–2). The hypostomal bridge is short (40,0), whereas it is long to very long (40,1) in other Chalcididae (Smicromorphinae excepted). The ata-pta intersection is far from the base of maxillary condyles (mc) (44,0), whereas it is close to mc (44,1) in the remaining species, but the plesiomorphic state also is observed in Phasgonophorinae. The propodeal spiracles are subcircular to elliptical (69,0), whereas they are slit-like in other species excepted in Tropimeriidini (69,1). The prosternum is rounded between the ventral and posterior surfaces (75,0), whereas it is angulate or carinate elsewhere, excepted in Smicromorphinae (75,1).

By contrast, Cratocentrinae included within the clade (Chalcidinae + Smicromorphinae + Dirihininae + Epitraninae + Brachymeriinae) as observed in the ASTRAL UCE tree is supported by only five characters: ventral margin of torulus not adjacent to clypeus (17,0) (this character state also occurs in Belaspidiini and Tropimeridinii and is homoplastic in Chalcidoidea); absence of a raised carina on the inner margin of axillula (65,0); ventral ornamentation of metafemur with large, regular, lobe like teeth (114,2) (however Dirhininae and Smicromorphinae have small teeth as in Haltichellinae); basal tooth of metafemur near base of femur (115,0) (character state also present in Notaspidiini); apex of metatibia diagonally truncate (118,1).

Thus, morphological data provide more support for Cratocentrinae as sister to all other Chalcididae. Besides, a scenario of loss and reacquisition of the head characters implied by the ASTRAL UCE tree seems unlikely. Consequently, the position of Cratocentrinae as sister to all other Chalcididae is globally better supported by our molecular and morphological analyses.

One question still remains unanswered: how can we explain that Cratocentrinae are nested within Chalcididae in the ASTRAL UCE tree? It is difficult to draw firm conclusions regarding this point. Our analyses suggest that individual UCE trees are insufficiently resolved to allow a proper inference on the position of the outgroups from all bipartitions present in the input gene trees. Indeed, a majority of trees with intermixed outgroups and ingroups can complicate species tree inferences (Mai et al., 2017). The consequence of this lack of information is that outgroups are placed in an intermediate position. Indeed, the position of the outgroups in the ASTRAL tree corresponds to a mid-point rooting of the ML trees (Fig. S1C) and topology C is recovered by ASTRAL when the set of input trees is reduced to those for which the ingroup is monophyletic. Outgroup choice is a difficult decision. Ideally, outgroups should be as close as possible to the ingroups to reduce LBA artefact while remaining sufficiently distantly related to reduce impacts of ILS. However, an informed choice is often difficult if not impossible for hyperdiverse and poorly known groups.

Bringing together all species for phylogenetic inference also is impossible and such large datasets would be impossible to analyze with current methods (Philippe et al., 2017). This is why exploration of phylogenetic incongruence and systematic bias is particularly necessary. Further research is needed to better understand possible drawbacks of tree reconciliation methods based on gene tree topology when they are used on UCEs and what could be the best strategy for alignment cleaning to preserve signal contained in gaps (Donath and Stadler, 2018).

Position of Chalcidinae. Our results suggest that the position of Chalcidinae as sister to Haltichellinae in the UCE ML trees could result from a GC content bias. The largest difference between the observed GC content and that predicted under the substitution model is obtained for GC-rich UCEs. In addition, GGI analyses show that topology A is preferred by UCEs with a significantly higher GC content (Fig. 9). Furthermore, hierarchical clustering of taxa based on their GC content shows that some Haltichellinae share more similar GC content with Chalcidinae or other subfamilies than with members of their own subfamily. GC-rich markers are more subject to recombination (Lartillot et al., 2007; Romiguier and Roux, 2017) and, as a consequence, to ILS (Pease and Hahn, 2013). Thus, it is not surprising that only methods that are statistically consistent under the multispecies coalescent model (i.e. ILS-aware methods ASTRAL, ASTRID) do not recover Chalcidinae as sister to Haltichellinae from the analysis of the complete dataset. ILS-aware methods have indeed been developed primarily to solve the deepest relationships for rapid radiations (e.g. birds: Mirarab et al., 2014a; Mirarab et al., 2014c). For the concatenation approach, when the most GC-biased UCEs (GC content >0.48; *c*. 28% of the total UCEs which corresponds to 23.7% of the total sites) or nucleotide sites (GC content >0.57; 18.9% of the total sites) were removed, a sister taxa relationship between Chalcidinae and the BDEPS clade (Brachymeriinae + Dirhininae + Epitraninae + Phasgonophorinae + Smicromorphinae) was inferred, albeit with moderate bootstrap support (Tables 3 and 4, Fig. 11, Appendix S1). This result agrees with other studies on reduced datasets, which revealed that UCEs can be GC-biased and support conflicting topologies (Sun et al., 2014; Bossert et al., 2017). However, we

encourage the removal of the most GC-biased nucleotide sites instead of the full UCEs to preserve phylogenetic signal in the analyzed subset. Furthermore, no morphological character supports a close relationship between Chalcidinae and Haltichellinae as observed in UCE ML trees, which confirms that this position is likely an artefact. Conversely, Chalcidinae as sister to the BDEPS clade (ASTRID) is supported by three characters: a single median carina between metacoxa (96,1); one apical spur on metatibia (119,1); absence of transverse carina in front of cercal plates (128,0).

Position of monotypic or species-poor groups (Zavoyini, Smicromorphinae). When it comes to the analysis of ancient groups that have undergone an explosive radiation as in Chalcidoidea (Heraty et al., 2013), another issue is the presence of monotypic or species-poor groups that are the only extant representatives of a long line of ancestors. These lineages are characterized by long external branches and insidious LBA artefacts may occur (not necessarily with the outgroups). On the morphological side, these taxa can be highly transformed and homologies between their features and those observed in the remaining species difficult to assess. Here, the position of two genera, *Zavoya* and *Smicromorpha,* remains ambiguous.

Position of Zavoyini. Contrary to the results from the UCEs, *Zavoya* (three species known) is strongly supported as sister to *Notaspidium* in the morphological tree, with which it shares a few characters (Fig. 10), although only one is an unambiguous synapomorphy (120,0). Additionally, this synapomorphy is a character loss (the ventral carinae of the metatibia are absent), that may confound interpretation of homology and relationships (Bleidorn, 2007). For all other characters the same character state is observed only in species that do not belong to the Haltichellinae in which *Zavoya* and *Notaspidium* are classified. These characters could thus be considered as local synapomorphies and, together with the absence of the ventral carinae on the metatibia, could reveal an undetected artefact in our UCE analysis that may be reduced with an increasing sampling of *Zavoya, Notaspidium* and Haltichellinae species. Further studies are nevertheless required to assess whether morphological convergence or systematic bias drive the position of *Zavoya*.

Position of Smicromorphinae. The position of *Smicromorpha* also is doubtful both in the morphological and the molecular trees. Even after UCE removal based on TreeShrink results (*Smicromorpha* is the most flagged taxon; Table S2), the long branch is still obvious (Appendix S1, Fig. 11). Smicromorphinae are highly transformed parasitoids of weaver-ant larvae (*Oecophylla*, Formicinae) and character homologies are difficult to assess. During the day or at dusk, female *Smicromorpha* deposit their eggs on silk-spinning larva of weaver ants held by workers to seal the leaves that are being pulled together by other workers when building their nest. Of the seven known species of *Smicromorpha*, two were reared from and three were collected flying around nests of *Oecophylla smaragdina* (Fabricius) in the Oriental and Australasian regions (Naumann, 1986; Darling, 2009). The biology of other species is unknown. Although there is no fossil record for *Smicromorpha*, multiple fossils of *Oecophylla* are known from Europe (Barden, 2017) suggesting that numerous species have become extinct since the Eocene epoch (the estimated age of the first fossil is *c*. 56 Ma). Interestingly, *Oecophylla* also is on a long branch and its putative relationships might therefore be artifactual (Ward et al., 2016). The highly specialized *Smicromorpha–Oecophylla* interaction and the numerous extinct lineages may explain the long branches and the difficulties encountered in correctly placing these taxa in phylogenies. Morphological data support a sister taxa relationship between *Smicromorpha*, Dirhininae and Epitraninae but this clade is not recovered in the UCE tree. Analysis of morphological character transformation (Appendix S3) and ancestral state reconstruction (Appendix S2) do not provide clear support toward a single hypothesis. Further studies are required to clarify the position of *Smicromorpha*. The addition of more species of *Smicromorpha* and the inclusion of an undescribed genus, the probable sister taxon of *Smicromorpha* in the Afrotropical region, that we unfortunately failed to sequence due to poor specimen preservation, may improve the results. However, all of these species are extremely rare and difficult to collect.

Relationships between Epitraninae and Dirhininae. Finally, a conflict also is observed between morphological and molecular data for Dirhininae and Epitraninae. These subfamilies are recovered as sister taxa in the morphological tree, whereas they are shown to be distantly related in the molecular trees. The sister taxa relationship is supported mostly by a closely related structure of the tentorium and other characters that are homoplastic especially those of the mesoscutellum, the forewings and the hind legs. Therefore, their close relationships in our morphological analysis may reflect convergence, but here again analysis of morphological character transformation (Appendix S3) and ancestral state reconstruction (Appendix S2) did not help to sort out among hypotheses.

Conclusion

The increasing use of high-throughput sequencing technologies combined with the decreasing number of taxonomists can result in a global overconfidence in phylogenetic hypotheses based on a large amount of molecular data. Furthermore, phylogenetic trees inferred from genome-scale data are usually highly supported which often is wrongly confused with accuracy, and falsely reinforces confidence in molecular results. Several authors have strongly advocated a systematic exploration of biases with different analytical methods. Indeed, this exploration may highlight better, alternative topologies that would not be revealed by a point-and-click approach. However, such studies are rare, especially when datasets are composed of hundreds of taxa and genes, which makes computation time prohibitive and incompatible with the current publish or perish system. A thorough exploration of phylogenetic tree space may nevertheless reveal alternative hypotheses that are difficult to rank without independent sources of evidence. Our study highlights the power of a systematic exploration of biases to sort among conflicting phylogenomic hypotheses and the usefulness of a careful analysis of morphological features by expert taxonomists to corroborate (or not) the most likely topology. It may provide guidelines to build the tree of life of other hyperdiverse groups of animals on which little phylogenetic knowledge has been acquired, which is the rule rather than the exception in nonvertebrate taxa.

Acknowledgements

We are grateful to Cedric Mariac and Leila Zekraoui (IRD, DIADE, France) for providing access to the Bioruptor; Audrey Weber (INRA, AGAP, France) for sequencing of the libraries and the Genotoul bioinformatics platform Toulouse Midi-Pyrenees, France for providing computing resources. We thank Natalie Dale-Skey Papilloud (NHM, London) and Nicole Fisher (ANIC, Canberra) for the loan of specimens as well as the Queensland government for collecting permits (WITK18248017-WITK18278817). We thank four anonymous reviewers for their careful review of the manuscript. This work is part of a large NSF project led by John Heraty (UC Riverside USA), Jim Woolley (Texas A&M University USA) and Matt Yoder (University of Illinois USA) that attempts to solve the phylogeny of the Chalcidoidea with NGS approaches and was funded by the INRA SPE department (recurrent funding to JYR and AC). USDA is an equal opportunity employer and provider. Trade names mentioned herein are for informational purposes only and do not imply endorsement by USDA.

Author contributions

JYR, AC and GD designed the study; JYR and AC obtained funding; GD, JYR, SF and SvN contributed samples; GD and JYR identified samples; SN, LS and SF performed laboratory work; BBB, MG and SB contributed sequences (USNM samples); SR wrote script to detect cross-contaminations; GD assembled the morphological matrix; JYR, GD and AC analyzed morphological data; AC and JYR analyzed molecular data; MC and JPR provided help with R; AC, JYR and GD drafted the manuscript; AC, JYR and GD reviewed the MS. All authors commented on the manuscript.

Data availability statement

Fastq paired reads for analyzed samples are available as a NCBI Sequence Read Archive (ID#PRJNA606284). Custom script to detect cross-contamination is available from https://github.com/DNAdiversity/UCE-Cross-Contamination-Check. Datasets (morphological matrix, concatenated UCEs) and trees have been uploaded on Zenodo (https://doi.org/10.5281/zenodo.3666638).

References

Abby, S.S., Tannier, E., Gouy, M. and Daubin, V., 2010. Detecting lateral gene transfers by statistical reconciliation of phylogenetic forests. BMC Bioinform. 11, 324.

Abul-Sood, M.I., Gadallah, N.S., Hossni, M.T. and Delvare, G., 2018. The subfamily Cratocentrinae (Hymenoptera: Chalcididae): reappraisal of their morphological characters and review of the West Palaearctic species, with the description of two new species. Zootaxa 4377, 490–516.

Andrews, S., 2010. FastQC - A Quality Control Application for FastQ Files. Available from http://www.bioinformatics.babraham.ac.uk/projects/fastqc/.

Arcila, D., Orti, G., Vari, R., Armbruster, J.W., Stiassny, M.L.J., Ko, K.D., Sabaj, M.H., Lundberg, J., Revell, L.J. and Betancur-R, R., 2017. Genome-wide interrogation advances resolution of recalcitrant groups in the tree of life. Nat. Ecol. Evol. 1, 20.

Barden, P., 2017. Fossil ants (Hymenoptera: Formicidae): ancient diversity and the rise of modern lineages. Myrmecol. News 24, 1–30.

Bergsten, J., 2005. A review of long-branch attraction. Cladistics 21, 163–193.

Betancur-R, R., Arcila, D., Vari, R.P., Hughes, L.C., Oliveira, C., Sabaj, M.H. and Orti, G., 2019. Phylogenomic incongruence, hypothesis testing, and taxonomic sampling: the monophyly of characiform fishes. Evolution 73, 329–345.

Blaimer, B.B., Brady, S.G., Schultz, T.R., Lloyd, M.W., Fisher, B.L. and Ward, P.S., 2015. Phylogenomic methods outperform traditional multi-locus approaches in resolving deep evolutionary history: a case study of formicine ants. BMC Evol. Biol. 15, 271.

Blaimer, B.B., LaPolla, J.S., Branstetter, M.G., Lloyd, M.W. and Brady, S.G., 2016a. Phylogenomics, biogeography and

diversification of obligate mealybug-tending ants in the genus *Acropyga*. Mol. Phylogenet. Evol. 102, 20–29.
Blaimer, B.B., Lloyd, M.W., Guillory, W.X. and Brady, S.G., 2016b. Sequence capture and phylogenetic utility of genomic ultraconserved elements obtained from pinned insect specimens. PLoS ONE 11, e0161531.
Bleidorn, C., 2007. The role of character loss in phylogenetic reconstruction as exemplified for the Annelida. J. Zool. Syst. Evol. Res. 45, 299–307.
Blomberg, S.P., Garland, J.T. and Ives, A.R., 2003. Testing for phylogenetic signal in comparative data: behavioral traits are more labile. Evolution 57, 717–745.
Bolger, A.M., Lohse, M. and Usadel, B., 2014. Trimmomatic: a flexible trimmer for Illumina sequence data. Bioinformatics 30, 2114–2120.
Borowiec, M.L., 2016. AMAS: a fast tool for alignment manipulation and computing of summary statistics. PeerJ 4, e1660.
Bossert, S. and Danforth, B.N., 2018. On the universality of target-enrichment baits for phylogenomic research. Methods Ecol. Evol. 9, 1453–1460.
Bossert, S., Murray, E.A., Blaimer, B.B. and Danforth, B.N., 2017. The impact of GC bias on phylogenetic accuracy using targeted enrichment phylogenomic data. Mol. Phylogenet. Evol. 111, 149–157.
Bossert, S., Murray, E.A., Almeida, E.A.B., Brady, S.G., Blaimer, B.B. and Danforth, B.N., 2019. Combining transcriptomes and ultraconserved elements to illuminate the phylogeny of Apidae. Mol. Phylogenet. Evol. 130, 121–131.
Bouček, Z., 1988. Australasian Chalcidoidea (Hymenoptera): a Biosystematic Revision of Genera of Fourteen Families, With a Reclassification of Species. CAB International, Wallingford, Oxon, UK.
Boussau, B., Walton, Z., Delgado, J.A., Collantes, F., Beani, L., Stewart, I.J., Cameron, S.A., Whitfield, J.B., Johnston, J.S., Holland, P.W.H. *et al*., 2014. Strepsiptera, phylogenomics and the Long Branch attraction problem. PLoS ONE 9, e107709.
Branstetter, M.G., Danforth, B.N., Pitts, J.P., Faircloth, B.C., Ward, P.S., Buffington, M.L., Gates, M.W., Kula, R.R. and Brady, S.G., 2017a. Phylogenomic insights into the evolution of stinging wasps and the origins of ants and bees. Curr. Biol. 27, 1019–1025.
Branstetter, M.G., Longino, J.T., Ward, P.S. and Faircloth, B.C., 2017b. Enriching the ant tree of life: enhanced UCE bait set for genome-scale phylogenetics of ants and other Hymenoptera. Methods Ecol. Evol. 8, 768–776.
Burks, R.A. and Heraty, J.M., 2015. Subforaminal bridges in Hymenoptera (Insecta), with a focus on Chalcidoidea. Arthropod Struct. Dev. 44, 173–194.
Burks, R.A., Heraty, J.M., Gebiola, M. and Hansson, C., 2011. Combined molecular and morphological phylogeny of Eulophidae (Hymenoptera: Chalcidoidea), with focus on the subfamily Entedoninae. Cladistics 27, 1–25.
Campbell, B., Heraty, J., Rasplus, J.Y., Chan, K., Steffan-Campbell, J. and Babcock, C., 2000. Molecular systematic of the Chalcidoidea using 28S-rDNA. In: Austin, A.D. and Dowton, M. (Eds.), The Hymenoptera: Evolution, Biodiversity and Biological Control. CSIRO Publishing, Canberra, pp. 59–73.
Chen, Y., Hui, X.A., Fu, J.Z. and Huang, D.W., 2004. A molecular phylogeny of eurytomid wasps inferred from DNA sequence data of 28S, 18S, 16S, and COI genes. Mol. Phylogenet. Evol. 31, 300–307.
Consoli, F.L., Parra, J.R.P. and Zucchi, R.A. (Eds), 2010. Egg Parasitoids in Agroecosystems with Emphasis on *Trichogramma*. Springer, Dordrecht.
Crotty, S.M., Minh, B.Q., Bean, N.G., Holland, B.R., Tuke, J., Jermiin, L.S. and Haeseler, A., 2019. GHOST: Recovering historical signal from heterotachously-evolved sequence alignments. Syst. Biol 69, 249–264.
Cruaud, A., Rønsted, N., Chantarasuwan, B., Chou, L.S., Clement, W., Couloux, A., Cousins, B., Forest, F., Genson, G., Harrison, R.D. *et al*., 2012. An extreme case of plant-insect co-diversification: figs and fig-pollinating wasps. Syst. Biol. 61, 1029–1047.
Cruaud, A., Nidelet, S., Arnal, P., Weber, A., Fusu, L., Gumovsky, A., Huber, J., Polaszek, A. and Rasplus, J.-Y., 2019. Optimised DNA extraction and library preparation for minute arthropods: application to target enrichment in chalcid wasps used for biocontrol. Mol. Ecol. Resour. 19, 702–710.
Darling, D.C., 2009. A new species of *Smicromorpha* (Hymenoptera, Chalcididae) from Vietnam, with notes on the host association of the genus. ZooKeys 20, 155–163.
Delvare, G., 1992. A reclassification of the Chalcidini with a checklist of the New World species. Memoirs Am. Entomol. Inst. 53, 119–466.
Delvare, G., 2017. Order Hymenoptera, family Chalcididae. Arthropod fauna UAE 6, 225–274.
Delvare, G. and Copeland, R.S., 2018. Four-horned wasps, description of some remarkable *Dirhinus* (Hymenoptera, Chalcididae) from Kenya, with a discussion of their taxonomic placement. Zootaxa 4374, 301–349.
Delvare, G., Ribes Escolà, A., Stojanova, A.M., Benoit, L., Lecomte, J. and Askew, R.R., 2019. Exploring insect biodiversity: the parasitic Hymenoptera, chiefly Chalcidoidea, associated with seeds of asphodels (Xanthorrhoeaceae), with the description of nine new species belonging to Eurytomidae and Torymidae. Zootaxa 4597, 1–90.
Desjardins, C.A., Regier, J.C. and Mitter, C., 2007. Phylogeny of pteromalid parasitic wasps (Hymenoptera : Pteromalidae): Initial evidence from four protein-coding nuclear genes. Mol. Phylogenet. Evol. 45, 454–469.
Dirzo, R., Young, H.S., Galetti, M., Ceballos, G., Isaac, N.J.B. and Collen, B., 2014. Defaunation in the Anthropocene. Science 345, 401–406.
Donath, A. and Stadler, P.F., 2018. Split-inducing indels in phylogenomic analysis. Algorithms Mol. Biol. 13, 12.
Duchêne, D.A., Bragg, J.G., Duchêne, S., Neaves, L.A., Potter, S., Moritz, C., Johnson, R.N., Ho, S.Y.W. and Eldridge, M.D.B., 2018. Analysis of phylogenomic tree space resolves relationships among marsupial families. Syst. Biol. 67, 400–412.
Ebach, M.C., Valdecasas, A.G. and Wheeler, Q.D., 2011. Impediments to taxonomy and users of taxonomy: accessibility and impact evaluation. Cladistics 27, 550–557.
Faircloth, B.C., McCormack, J.E., Crawford, N.G., Harvey, M.G., Brumfield, R.T. and Glenn, T.C., 2012. Ultraconserved elements anchor thousands of genetic markers spanning multiple evolutionary timescales. Syst. Biol. 61, 717–726.
Faircloth, B.C., Branstetter, M.G., White, N.D. and Brady, S.G., 2015. Target enrichment of ultraconserved elements from arthropods provides a genomic perspective on relationships among Hymenoptera. Mol. Ecol. Resour. 15, 489–501.
Foottit, R.G. and Adler, P.H. (Eds), 2009. Insect biodiversity: Science and Society. Wiley-Blackwell, West Sussex, UK.
Godfray, H.C.J., 1994. Parasitoids. Behavioral and Evolutionary Ecology. Princeton University Press, Princeton, NJ.
Gori, K., Suchan, T., Alvarez, N., Goldman, N. and Dessimoz, C., 2016. Clustering genes of common evolutionary history. Mol. Biol. Evol. 33, 1590–1605.
Gu, X., Fu, Y.X. and Li, W.H., 1995. Maximum likelihood estimation of the heterogeneity of substitution rate among nucleotide sites. Mol. Biol. Evol. 12, 546–557.
Guindon, S., Dufayard, J.F., Lefort, V., Anisimova, M., Hordijk, W. and Gascuel, O., 2010. New algorithms and methods to estimate maximum-likelihood phylogenies: assessing the performance of PhyML 3.0. Syst. Biol. 59, 307–321.
Gul, M.A., Soliman, A.M., Gadallah, N.S., Dhafer, H.M.A. and Delvare, G., in press. The genus Phasgonophora Westwood, 1832 (Hymenoptera, Chalcididae) in Saudi Arabia: re-evaluation of its limits and description of three new species from Saudi Arabia. Journal of Hymenoptera Research.
Haas, B.J., Papanicolaou, A., Yassour, M., Grabherr, M., Blood, P.D., Bowden, J., Couger, M.B., Eccles, D., Li, B., Lieber, M.

et al., 2013. De novo transcript sequence reconstruction from RNA-seq using the Trinity platform for reference generation and analysis. Nat. Protoc. 8, 1494–1512.

Hallmann, C.A., Sorg, M., Jongejans, E., Siepel, H., Hofland, N., Schwan, H., Stenmans, W., Müller, A., Sumser, H., Hörren, T. *et al*., 2017. More than 75 percent decline over 27 years in total flying insect biomass in protected areas. PLoS ONE 12, e0185809.

Heled, J. and Drummond, A.J., 2010. Bayesian inference of species trees from multilocus data. Mol. Biol. Evol. 27, 570–580.

Heraty, J.M., Burks, R.A., Cruaud, A., Gibson, G.A.P., Liljeblad, J., Munro, J., Rasplus, J.-Y., Delvare, G., Janšta, P., Gumovsky, A. *et al*., 2013. A phylogenetic analysis of the megadiverse Chalcidoidea (Hymenoptera). Cladistics 29, 466–542.

Hosner, P.A., Faircloth, B.C., Glenn, T.C., Braun, E.L. and Kimball, R.T., 2016. Avoiding missing data biases in phylogenomic inference: an empirical study in the landfowl (Aves: Galliformes). Mol. Biol. Evol. 33, 1110–1125.

Janšta, P., Cruaud, A., Delvare, G., Genson, G., Heraty, J., Křížková, B. and Rasplus, J.-Y., 2018. Torymidae (Hymenoptera, Chalcidoidea) revised: molecular phylogeny, circumscription and reclassification of the family with discussion of its biogeography and evolution of life-history traits. Cladistics 34, 627–651.

Jesovnik, A., Sosa-Calvo, J., Lloyd, M.W., Branstetter, M.G., Fernandez, F. and Schultz, T.R., 2017. Phylogenomic species delimitation and host-symbiont coevolution in the fungus-farming ant genus *Sericomyrmex* Mayr (Hymenoptera: Formicidae): ultraconserved elements (UCEs) resolve a recent radiation. Syst. Entomol. 42, 523–542.

Kassambara, A. and Mundt, F.,2017. factoextra: extract and visualize the results of multivariate data analyses. R package version, 1.0.5. https://CRAN.R-project.org/package=factoextra

Katoh, K. and Standley, D.M., 2013. MAFFT multiple sequence alignment software version 7: improvements in performance and usability. Mol. Biol. Evol. 30, 772–780.

Kaufman, L. and Rousseeuw, P.J., 1990. Partitioning around medoids (Program PAM). In: Kaufman, L. and Rousseeuw, P.J. (Eds.) Finding Groups in Data: An Introduction to Cluster Analysis. John Wiley & Sons Inc., Hoboken, NJ, pp. 68–125.

Kieran, T.J., Gordon, E.R.L., Forthman, M., Hoey-Chamberlain, R., Kimball, R.T., Faircloth, B.C., Weirauch, C. and Glenn, T.C., 2019. Insight from an ultraconserved element bait set designed for hemipteran phylogenetics integrated with genomic resources. Mol. Phylogenet. Evol. 130, 297–303.

Kumar, S., Filipski, A.J., Battistuzzi, F.U., Pond, S.L.K. and Tamura, K., 2012. Statistics and truth in phylogenomics. Mol. Biol. Evol. 29, 457–472.

Lanfear, R., Frandsen, P.B., Wright, A.M., Senfeld, T. and Calcott, B., 2017. PartitionFinder 2: new methods for selecting partitioned models of evolution for molecular and morphological phylogenetic analyses. Mol. Biol. Evol. 34, 772–773.

Lartillot, N., Brinkmann, H. and Philippe, H., 2007. Suppression of long-branch attraction artefacts in the animal phylogeny using a site-heterogeneous model. BMC Evol. Biol. 7, S4.

Lemmon, A.R., Brown, J.M., Stanger-Hall, K. and Lemmon, E.M., 2009. The effect of ambiguous data on phylogenetic estimates obtained by maximum likelihood and Bayesian inference. Syst. Biol. 58, 130–145.

Lotfalizadeh, H., Delvare, G. and Rasplus, J.Y., 2007. Phylogenetic analysis of Eurytominae based on morphological characters (Chalcidoidea: Eurytomidae). Zool. J. Linn. Soc. 151, 441–510.

Maddison, W.P. andMaddison, D.R.,2018. Mesquite: a modular system for evolutionary analysis. Available at http://mesquite project.org

Maechler, M., Rousseeuw, P., Struyf, A., Hubert, M. and Hornik, K.2018. cluster: Cluster Analysis Basics and Extensions. R package version 2.0.7-1.

Magoc, T. and Salzberg, S.L., 2011. FLASH: fast length adjustment of short reads to improve genome assemblies. Bioinformatics 27, 2957–2963.

Mai, U. and Mirarab, S., 2018. TreeShrink: fast and accurate detection of outlier long branches in collections of phylogenetic trees. BMC Genom. 19, 272.

Mai, U., Sayyari, E. and Mirarab, S., 2017. Minimum variance rooting of phylogenetic trees and implications for species tree reconstruction. PLoS ONE 12, e0182238.

McCormack, J.E., Faircloth, B.C., Crawford, N.G., Gowaty, P.A., Brumfield, R.T. and Glenn, T.C., 2012. Ultraconserved elements are novel phylogenomic markers that resolve placental mammal phylogeny when combined with species-tree analysis. Genome Res. 22, 746–754.

McCormack, J.E., Tsai, W.L.E. and Faircloth, B.C., 2016. Sequence capture of ultraconserved elements from bird museum specimens. Mol. Ecol. Resour. 16, 1189–1203.

Minh, B.Q., Nguyen, M.A.T. and von Haeseler, A., 2013. Ultrafast approximation for phylogenetic bootstrap. Mol. Biol. Evol. 30, 1188–1195.

Mirarab, S., Bayzid, M.S., Boussau, B. and Warnow, T., 2014a. Statistical binning enables an accurate coalescent-based estimation of the avian tree. Science 346, 1250463.

Mirarab, S., Nguyen, N. and Warnow, T., 2014b. PASTA: ultra-large multiple sequence alignment. Res. Comput. Mol. Biol. 22, 177–191.

Mirarab, S., Reaz, R., Bayzid, M.S., Zimmermann, T., Swenson, M.S. and Warnow, T., 2014c. ASTRAL: genome-scale coalescent-based species tree estimation. Bioinformatics 30, i541–i548.

Munro, J.B., Heraty, J.M., Burks, R., Hawks, D., Cruaud, A., Rasplus, J.-Y. and Janšta, P., 2011. A molecular phylogeny of the Chalcidoidea (Hymenoptera). PLoS ONE 6, e27023.

Murray, E.A., Carmichael, A.E. and Heraty, J.M., 2013. Ancient host shifts followed by host conservatism in a group of ant parasitoids. Proc. R. Soc. B Biol. Sci. 280, 20130495.

Naumann, I.D., 1986. A revision of the Indo-Australian Smicromorphinae (Hymenoptera: Chalcididae). Mem. Queensl. Mus. 22, 169–187.

Nguyen, L.T., Schmidt, H.A., von Haeseler, A. and Minh, B.Q., 2015. IQ-TREE: A fast and effective stochastic algorithm for estimating maximum likelihood phylogenies. Mol. Biol. Evol. 32, 268–274.

van Noort, S. and Compton, S.G., 1996. Convergent evolution of Agaoninae and Sycoecinae (Agaonidae, Chalcidoidea) head shape in response to the constraints of host fig morphology. J. Biogeogr. 23, 415–424.

Noyes, J.S.2019. Universal Chalcidoidea Database. World Wide Web electronic publication. http://www.nhm.ac.uk/chalcidoids (accessed December 2019).

Nute, M., Chou, J., Molloy, E.K. and Warnow, T., 2018. The performance of coalescent-basedspecies tree estimation methods under modelsof missing data. BMC Genom. 19, 286.

Owen, A.K., George, J., Pinto, J.D. and Heraty, J.M., 2007. A molecular phylogeny of the Trichogrammatidae (Hymenoptera : Chalcidoidea), with an evaluation of the utility of their male genitalia for higher level classification. Syst. Entomol. 32, 227–251.

Pease, J.B. and Hahn, M.W., 2013. More accurate phylogenies inferred from low recombination regions in the presence of incomplete lineage sorting. Evolution 67, 2376–2384.

Peterson, B.G. and Carl, P.,2018. PerformanceAnalytics: econometric tools for performance and risk analysis. R package version 1.5.2. https://CRAN.R-project.org/package=PerformanceAnalytics.

Philippe, H., Delsuc, F., Brinkmann, H. and Lartillot, N., 2005. Phylogenomics. Annu. Rev. Ecol. Evol. Syst. 36, 541–562.

Philippe, H., de Vienne, D.M., Ranwez, V., Roure, B., Baurain, D. and Delsuc, F., 2017. Pitfalls in supermatrix phylogenomics. Eur. J. Taxonomy 283, 1–25.

Phillips, M.J., Delsuc, F. and Penny, D., 2004. Genome-scale phylogeny and the detection of systematic biases. Mol. Biol. Evol. 21, 1455–1458.

Prathapan, D.K., Pethiyagoda, R., Bawa, K.S., Raven, P.H., Dharma Rajan, P. and 172 co-signatories from 35 countries,

(2018) When the cure kills—CBD limits biodiversity research. National laws fearing biopiracy squelch taxonomy studies. Science 360, 1405–1406.
Prebus, M., 2017. Insights into the evolution, biogeography and natural history of the acorn ants, genus *Temnothorax* Mayr (Hymenoptera: Formicidae). BMC Evol. Biol. 17, 250.
R Core Team, 2018. R version 3.5.1 (Feather Spray): A Language and Environment for Statistical Computing. R Foundation for Statistical Computing, Vienna, Austria. https://www.R-project.org/
Revell, L.J., 2012. Phytools: An R package for phylogenetic comparative biology (and other things). Methods Ecol. Evol. 3, 217–223.
Romiguier, J. and Roux, C., 2017. Analytical biases associated with GC-content in molecular evolution. Front. Genet. 8, 16.
Seo, T.K., 2008. Calculating bootstrap probabilities of phylogeny using multilocus sequence data. Mol. Biol. Evol. 25, 960–971.
Shimodaira, H., 2002. An approximately unbiased test of phylogenetic tree selection. Syst. Biol. 51, 492–508.
Shimodaira, H. and Hasegawa, M., 2001. CONSEL: for assessing the confidence of phylogenetic tree selection. Bioinformatics 17, 1246–1247.
Snodgrass, R.E., 1928. Morphology and evolution of the insect head and its appendages. Smithsonian Miscellaneous Collect. 80, 1–158.
Snodgrass, R.E., 1942. The skeleto-muscular mechanisms of the honeybee. Smithsonian Miscellaneous Collect. 103, 1–120.
Snodgrass, R.E., 1960. Facts and theories concerning the insect head. Smithsonian Miscellaneous Collections 142, 1–61.
Stamatakis, A., 2014. RAxML version 8: a tool for phylogenetic analysis and post-analysis of large phylogenies. Bioinformatics 30, 1312–1313.
Steffan, J.R., 1957. Morphologie du pétiole abdominal des Chalcididae (Hymenoptera). Bull. Mus. natl. hist. nat. 29, 315–322.
Stöver, B.C. and Müller, K.F., 2010. TreeGraph 2: Combining and visualizing evidence from different phylogenetic analyses. BMC Bioinform. 11, 7.
Streicher, J.W., Schulte, J.A. and Wiens, J.J., 2016. How should genes and taxa be sampled for phylogenomic analyses with missing data? An empirical study in iguanian lizards. Syst. Biol. 65, 128–145.
Struck, T.H., 2014. TreSpEx - detection of misleading signal in phylogenetic reconstructions based on tree information. Evol. Bioinform. 10, 51–67.
Sun, K.P., Meiklejohn, K.A., Faircloth, B.C., Glenn, T.C., Braun, E.L. and Kimball, R.T., 2014. The evolution of peafowl and other taxa with ocelli (eyespots): a phylogenomic approach. Proc. R. Soc. B Biol. Sci. 281, 20140823.
Swofford, D.L., 2003. PAUP*. Phylogenetic Analysis Using Parsimony (*and Other Methods). Version 4. Sinauer Associates, Sunderland, MA.
Swofford, D.L., Olsen, G.J., Waddell, P.J. and Hillis, D.M., 1996. Phylogenetic inference. In: Hillis, D.M., Moritz, C. and Mable, B.K. (Eds.) Molecular systematics. Sinauer Associates, Sunderland, MA, pp. 407–514.
Szöllősi, G.J. and Daubin, V., 2012. Modeling gene family evolution and reconciling phylogenetic discord. Methods Mol. Biol. 856, 29–51.
Tagliacollo, V.A., Lanfear, R. and Townsend, J., 2018. Estimating improved partitioning schemes for ultraconserved elements. Mol. Biol. Evol. 35, 1798–1811.
Titley, M.A., Snaddon, J.L. and Turner, E.C., 2017. Scientific research on animal biodiversity is systematically biased towards vertebrates and temperate regions. PLoS ONE 12, e0189577.
Vachaspati, P. and Warnow, T., 2015. ASTRID: Accurate Species TRees from Internode Distances. BMC Genom. 16(Suppl. 10), S3.
Van Dam, M.H., Lam, A.W., Sagata, K., Gewa, B., Laufa, R., Balke, M., Faircloth, B.C. and Riedel, A., 2017. Ultraconserved elements (UCEs) resolve the phylogeny of Australasian smurf-weevils. PLoS ONE 12, e0188044.
Vilhelmsen, L., 1999. The occipital region in the basal Hymenoptera (Insecta): a reappraisal. Zoolog. Scr. 28, 75–85.
Vilhelmsen, L., 2011. Head capsule characters in the Hymenoptera and their phylogenetic implications. ZooKeys 130, 343–361.
Wägele, H., Klussmann-Kolb, A., Kuhlmann, M., Haszprunar, G., Lindberg, D., Koch, A. and Wägele, J.W., 2011. The taxonomist - an endangered race. A practical proposal for its survival. Front. Zool. 8, 25.
Ward, P.S. and Branstetter, M.G., 2017. The acacia ants revisited: convergent evolution and biogeographic context in an iconic ant/plant mutualism. Proc. R. Soc. B Biol. Sci. 284, 20162569.
Ward, P.S., Blaimer, B.B. and Fisher, B.L., 2016. A revised phylogenetic classification of the ant subfamily Formicinae (Hymenoptera: Formicidae), with resurrection of the genera *Colobopsis* and *Dinomyrmex*. Zootaxa 4072, 343–357.
Wickham, H., 2016. ggplot2: Elegant Graphics for Data Analysis. Springer, New York, NY.
Wiens, J.J., 2003. Missing data, incomplete taxa, and phylogenetic accuracy. Syst. Biol. 52, 528–538.
Wiens, J.J., 2004. The role of morphological data in phylogeny reconstruction. Syst. Biol. 53, 653–661.
Wiens, J.J. and Morrill, M., 2011. Missing data in phylogenetic analysis: reconciling results from simulations and empirical data. Syst. Biol. 60, 719–731.
Wijesekara, G.A.W., 1997a. Generic relationships within the tribes Cratocentrini and Phasganophorini (Hymenoptera: Chalcididae). J. Hymenoptera Res. 6, 297–335.
Wijesekara, G.A.W., 1997b. Phylogeny of Chalcididae (Insecta: Hymenoptera) and its congruence with contemporary hierarchical classification. Contrib. Am. Entomol. Inst. 29, 1–61.
Zhang, C., Rabiee, M., Sayyari, E. and Mirarab, S., 2018. ASTRAL-III: polynomial time species tree reconstruction from partially resolved gene trees. BMC Bioinform. 19, 153.
Zhong, B. and Betancur-R, R., 2017. Expanded taxonomic sampling coupled with gene genealogy interrogation provides unambiguous resolution for the evolutionary root of angiosperms. Genome Biol. Evol. 9, 3154–3161.
Zhu, Q.,2014. AfterPhylo. A Perl script for manipulating trees after phylogenetic reconstruction. Available from:https://github.com/qiyunzhu/AfterPhylo/.
Zimmermann, D. and Vilhelmsen, L., 2016. The sister group of Aculeata (Hymenoptera) – evidence from internal head anatomy, with emphasis on the tentorium. Arthropod Syst. Phylo. 74, 195–218.

Supporting Information

Additional supporting information may be found online in the Supporting Information section at the end of the article.

Figure S1. RAxML tree, complete UCE dataset.

Figure S2. IQTREE tree, complete UCE dataset.

Figure S3. ASTRAL tree, complete UCE dataset.

Figure S4. ASTRID tree, complete UCE dataset.

Figure S5. PAM clustering of the 538 UCE trees.

Figure S6. Correlation analysis for the properties of the UCEs (Spearman rank-based correlation).

Figure S7. Dendrogram of samples based on GC content of UCEs.

Figure S8. Phylogenetic trees inferred from the morphological matrix.

Table S1. Samples used in this study, results of the UCE-enrichment experiment and taxon properties in the concatenated dataset.

Table S2. UCEs in which samples were detected as outlier long branches by TreeShrink (b = 20).

Table S3. Properties of the analyzed UCEs and results of the Gene Genealogy Interrogation approach.

Table S4. Properties of the analyzed taxa in the different UCEs (GC content and LB scores).

Appendix S1. Trees obtained from the analysis of the UCE and morphological datasets. This file may be opened in e.g. Figtree to navigate between trees.

Appendix S2. Morphological matrix and ancestral state reconstruction for each character on the four competing topologies. This file can be opened with Mesquite to visualize character states, ancestral state reconstruction and CI/RI of the different characters.

Appendix S3. This Appendix describes the result of character mapping with PAUP* on the four topologies.

Appendix S4. Diagnoses of the family, subfamilies and tribes.